[116] Snigirev A., Kohn V., Snigireva I. and Lengeler B., *Nature* **384**, 49 (1996).
[117] Snigirev A., Kohn V., Snigireva I., Souvorov A. and Lengeler B., *Appl. Optics* **37**(4), 653 (1998).
[118] Snigirev A., Filseth B., Elleaume P., Klocke T., Kohn V., Lengeler B., Snigireva I., Soukorov A. and Tümmler J., Refractive lenses with high energy X-ray focusing, in: *High Heat Flux Engineering IV* (A. Khounsary, Ed.), Proc. SPIE **3151A** (1997).
[119] Lengeler, B., Tümmler, J., Snigireva, I.I. and Raven, C., *J. Appl. Phys.* **84**, 5855 (1998).

2 INTERACTION OF X-RAYS WITH MATTER

J.E. Fernández

National Institute of Physics of Matter (INFM) and Laboratory of Montecuccolino, University of Bologna, Italy

2.1 Introduction

X-rays are electromagnetic radiation with wavelengths around 100 pm which, upon interaction with matter (atoms), produce secondary radiation that carries useful information about the atoms comprising the target. As X-rays are very penetrating they probe the depth of the target, sampling an important volume. When an X-ray beam passes through an absorber it suffers attenuation, the degree of which depends on different types of absorption and scattering processes. In general, the Beer–Lambert law establishes that *equal paths into the same medium attenuate equal fractions of radiation.* Thus, for a path of length dx the intensity I will be reduced by dI, i.e.

$$\frac{dI}{I} = -\mu_L dx \tag{2.1}$$

where μ_L is called the linear attenuation coefficient, a magnitude characteristic of the medium and, for an homogeneous material, only a function of the energy. Eqn (2.1) has the well-known exponential solution

$$I(x) = I_0 e^{-\mu_L x} \tag{2.2}$$

with I_0 representing the intensity at $x = 0$.

Because the linear attenuation coefficient depends on the density of the medium, it is useful to define a mass attenuation coefficient μ which does not depend on the state of aggregation of the medium. Assuming that ρ is the density of the material, a mass element $dm = \rho dx$ g cm^{-2} corresponds to the path length dx. In this layer, Eqn (2.1) can be rewritten as

$$\frac{dI}{I} = -\mu dm = -\mu\rho dx \tag{2.3}$$

with the equivalent solution

Microscopic X-ray Fluorescence Analysis. Edited by Koen H.A. Janssens, Freddy C.V. Adams and Anders Rindby © 2000 John Wiley & Sons Ltd. ISBN 0-471-97426-9.

$$I(x) = I_0 e^{-\mu\rho x} \tag{2.4}$$

Obviously, $\mu = \mu_L/\rho$ is a property of the substance. For a mixture of substances with individual mass attenuation coefficients μ_i and weight fractions W_i, the mass attenuation coefficient of the compound is given by

$$\mu(\text{compound}) = \sum_i w_i \mu_i \tag{2.5}$$

The validity of the above expression is related to the absence of structure effects, i.e. when the interacting atoms can be considered isolated systems and a compound, a mixture of isolated atoms. Thus, this approximation is known as the isolated atoms approximation.

We can express the intensity equation in terms of the atomic attenuation coefficient, i.e. a coefficient which depends on the number of atoms as $dn = dm/atom\ mass = dm/(A/N) = (\rho N/A)dx$ along the path dx :

$$\frac{dI}{I} = -\mu_a dn = -\mu_a \frac{\rho N}{A} dx \tag{2.6}$$

with the obvious solution

$$I(x) = I_0 e^{-\mu_a \frac{\rho N}{A} x} \tag{2.7}$$

In Eqn (2.6), A represents the atomic weight and N is Avogadro's number. The atomic attenuation coefficient, in units of cm^2 or barns ($= 10^{-24} cm^2$), is the usual choice with which to describe the physics of the interactions.

2.2 Relevant aspects of photon interactions with matter

Photons can interact with matter in different ways depending on their energy [1–3]. The photons in the X-ray regime interact with the electron shells which surround the nucleus. The nucleus itself does not contribute to the scattering or absorption of photons.

The interaction of a photon of energy $h\nu$ with an isolated atom A has the effect of changing the atom's state from $|i\rangle$ to $|f\rangle$, which can be expressed as

$$A_i + h\,\nu_i \rightarrow A_f + h\,\nu_f \tag{2.8}$$

Equation (2.8) denotes the type of photon–atom interactions of interest in this work, having one initial photon and only one resulting photon. The term A_f denotes the atom plus all the non-photonic particles produced in the reaction.

There are three photon–atom processes whose influence prevail in the X-ray regime: the photoelectric effect in which the photons cause the ejection of an electron leaving a hole in the atom which, when the vacancy is filled by another electron, emits a fluorescence photon having the energy difference between the electron and the hole level; the unmodified or Rayleigh scattering

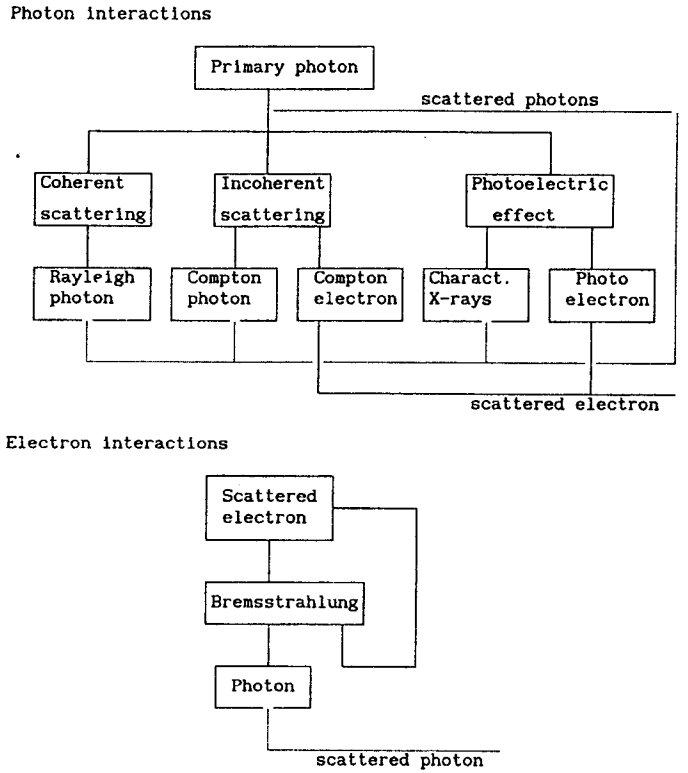

Figure 2.1 Main mechanisms of photon and electron scattering in the X-ray regime. Scattered electrons feed back new photons into the photon interactions cycle and, therefore, the full transport problem should be solved with two coupled systems of transport equations – one for polarized photons and one for polarized electrons. The photon transport equation (2.69), which neglects the electron interactions, is an excellent approximation when the probability for *bremsstrahlung* is low.

in which the photon changes momentum but not energy; and the modified or Compton scattering in which both momentum and energy are transferred to the electrons comprising the atom (Figure 2.1).

What we call an interaction may not be strictly a single process. Any sequence of physical processes in rapid succession, originated by a photon and producing one or more other photons, can be statistically considered as a unique interaction, as occurs for example with the photoelectric effect.

The resulting (or secondary) photon from the interactions may collide in turn with another atom, starting a multiple chain of events that we want to study. However, not only photons are produced in the photon–atom interactions. The photoelectric effect and the modified scattering produce electrons which, obeying other kinds of interactions, can produce new photons. As these

contributions render the transport problem far more complicated, because of the coupling between photons and electrons, we shall neglect in this work *bremsstrahlung* (braking radiation) of the Compton and photoelectric electrons, and also other photon sources such as anomalous scattering and pair production–annihilation.

The above-described interactions can be mathematically characterized by the probability density functions (or single-process kernels) changing the phase space coordinates of the photon during an interaction process, as defined in the following sections.

2.3 Single-process kernels

Single-process kernels play a very important role in transport theory. They represent the probability density – by unit wavelength, by unit solid angle, and by unit path – that the process may change, with the phase-space variables moving from $(\vec{\omega}', \lambda')$ to $(\vec{\omega}, \lambda)$. Here $\vec{\omega}', \vec{\omega}$ are the unit vectors defining the direction of propagation of the photon and λ', λ the wavelengths before and after a given interaction, respectively.

Therefore a *kernel* is directly related to the *double-differential scattering coefficient* of the interaction, i.e.

$$k_T(\vec{\omega}, \lambda, \vec{\omega}', \lambda') = \frac{d\sigma_T}{d\omega d\lambda} \tag{2.9}$$

Thus, the scattering coefficient for the process T can be obtained from

$$\sigma_T(\vec{\omega}', \lambda') = \int_0^\infty d\lambda \int_{4\pi} d\omega k_T(\vec{\omega}, \lambda, \vec{\omega}', \lambda') \tag{2.10}$$

allowing comparison with experimental or theoretical data. The photon cross-sections for the interaction processes of interest constitute the main part of the total attenuation coefficient [4–9], so we can define the total attenuation coefficient μ as

$$\mu = \sigma_C + \sigma_R + \tau \tag{2.11}$$

where σ_C and σ_R are the Compton (incoherent) and Rayleigh (coherent) integral attenuation coefficients and τ is the photoelectric attenuation coefficient (Figure 2.2).

If we consider the attenuation of photons, then at low energies the atomic photoelectric effect predominates, whereas at intermediate energies Compton scattering dominates. However, if we are concerned with the scattering of photons, then Rayleigh scattering dominates at low energies or forward angles, whereas Compton scattering dominates at higher energies or larger angles.

In what follows, the mathematical representation of a photon beam having a general state of polarization is presented first, followed by the definition of the atomic interaction kernels for the three dominating processes that participate in

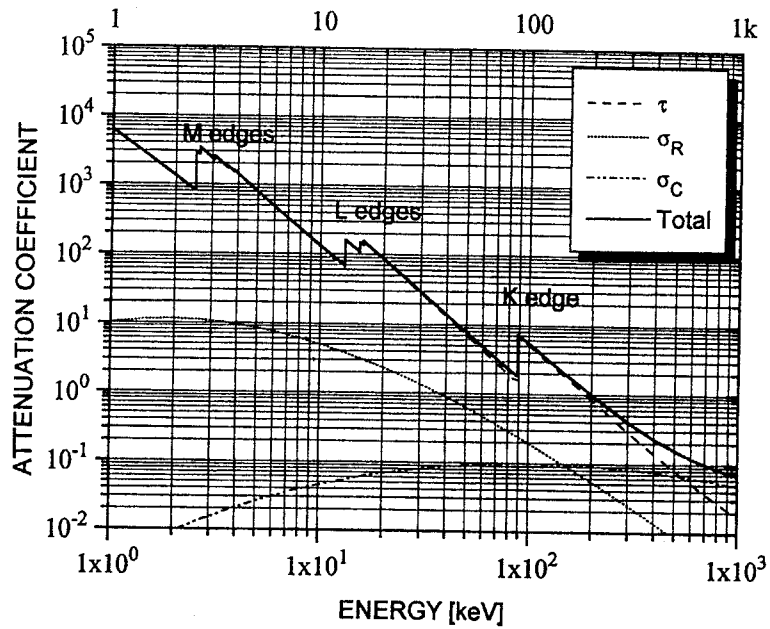

Figure 2.2 Plot of the total attenuation coefficient of Pb showing the contribution of the photoelectric, Rayleigh and Compton attenuation coefficients. Data taken from Ref. 4.

X-ray photon transport. These kernels are given for both average (scalar kernels) and generally polarized transport models (vector kernels). As a first approximation the coherent and incoherent scattering factor approximation is used to describe scattering cross-sections. The scattering factor approximation assumes a smooth behavior of the scattering cross-sections so they cannot explain scattering resonances [10] such as anomalous scattering [11, 12]. The effect of the relative motion of the electrons with respect to the incident photon beam will be considered later. The relative motion of the electrons does not have a significant effect on the coherent scattering. However, at least for the incoherent case, the scattering factor can be obtained with an integration of momentum profiles of single orbitals, giving a simple connection between the Compton profiles and the corresponding scattering factor [13]. Polarization effects will be also considered, and will be discussed separately for every scattering process.

2.3.1 REPRESENTATION OF POLARIZED RADIATION WITH THE STOKES PARAMETERS

The polarization of X-rays, a net wave effect, requires four parameters. The first parameter is *the beam intensity* and it is the only one considered in scalar

transport models. At each space point, for a given wavelength and direction of propagation, the most general beam of X-rays can be regarded as a mixture of elliptically polarized and unpolarized X-rays. The second parameter is the fraction of polarized X-rays (i.e. *the degree of polarization.*) The remaining two parameters describe the ellipse associated with the elliptically polarized component. One specifies the angle between the major axis of the ellipse and a fixed coordinate axis in space. This is generally referred to as *the orientation of the ellipse of polarization*. The other is the *ellipticity* of the ellipse, i.e. the ratio of the two axes of the ellipse. Because of the diverse nature of these four quantities, it is convenient to use an equivalent set, introduced by Sir George Stokes (1852), which contains all the physical information about the polarization state of the X-ray beam [14]. In this way, the photon transport can be described using a four-component parameterization obeying a vector transport equation. In this representation, a polarized beam of X-rays needs four parameters I_I, I_Q, I_U and I_V (the Stokes parameters, having the dimension of intensity) to specify the intensity, the degree of polarization, the orientation and the ellipticity of the ellipse of polarization, at each point of the space and in any given direction (Figure 2.3).

The Stokes intensities can be expressed in terms of the angles χ (the rotation of the major axis of the polarization ellipse about a direction parallel to the scattering plane) and β (which is related to the major-to-minor axes ratio or ellipticity). The meaning of these parameters become apparent from the relationships

$$I_Q = I_I \cos 2\beta \cos 2\chi \tag{2.12}$$

$$I_U = I_I \cos 2\beta \sin 2\chi \tag{2.13}$$

$$I_V = I_I \sin 2\beta \tag{2.14}$$

The Stokes components for an unpolarized beam are simply $(I_I, 0, 0, 0)$. For elliptically polarized X-rays we note that

$$\sin 2\beta = \frac{I_V}{I_I} \tag{2.15}$$

$$\tan 2\chi = \frac{I_U}{I_Q} \tag{2.16}$$

and the Stokes parameters satisfy the relationship

$$I_I^2 = I_Q^2 + I_U^2 + I_V^2 \tag{2.17}$$

Consequently, only three of the four parameters are independent.

For partially polarized X-rays (i.e. a mixture of unpolarized and elliptically polarized X-rays), all four parameters are necessary and the following relationship holds:

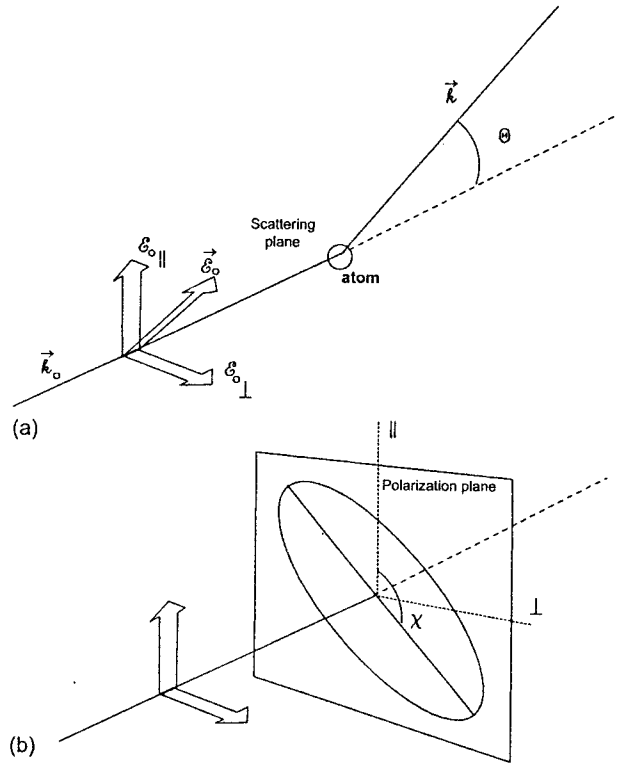

Figure 2.3 Graphical representation of the electric field vector of a polarized photon beam. (a) The scattering geometry determines the scattering plane, used as a reference frame. The electric field can be resolved in the parallel and normal directions to this plane. (b) The electric field vector lies on the polarization plane, which is normal to the propagation direction. The most general pure state of polarization of the photon beam is elliptical polarization. This means that the tip of the electric vector describes an ellipse on the polarization plane during the propagation. A linearly polarized beam is obtained as a limiting case by setting the length of the minor axis of the ellipse to zero. In that case, the angle χ represents the orientation of the line along which the electric field changes its amplitude periodically.

$$I_I^2 \geq I_Q^2 + I_U^2 + I_V^2 \tag{2.18}$$

Clearly the total intensity I_I and the additional parameters I_Q, I_U and I_V, completely determine, from an experimental point of view, the characteristics of an arbitrary beam. That is, two beams with the same Stokes parameters are optically equivalent as they cannot be distinguished experimentally.

A general beam of X-rays (with components (I_I, I_Q, I_U, I_V)) can be decomposed into two independent beams, one unpolarized and the other elliptically polarized, with their states of polarization defined by

$$\left(I_I^2 - \left(I_Q^2 + I_U^2 + I_V^2\right)^{1/2}, 0, 0, 0\right); \text{(unpolarized)} \tag{2.19}$$

$$\left(\left(I_Q^2 + I_U^2 + I_V^2\right)^{1/2}, I_Q, I_U, I_V\right); \text{(elliptically polarized)} \tag{2.20}$$

where β and χ are given by the relationships

$$\sin 2\beta = \frac{I_V}{(I_Q^2 + I_U^2 + I_V^2)^{1/2}} \tag{2.21}$$

$$\tan 2\chi = \frac{I_U}{I_Q} \tag{2.22}$$

It is customary to define the degree of polarization P as the fraction of polarized (scattered) radiation after the collision, which in terms of the Stokes intensities is given by

$$P = \frac{(I_Q^2 + I_U^2 + I_V^2)^{1/2}}{I_I} \tag{2.23}$$

It can be easily shown that the general beam can be written as

$$\begin{pmatrix} I_I \\ I_Q \\ I_U \\ I_V \end{pmatrix} = I_I \left\{ (1-P) \begin{pmatrix} 1 \\ 0 \\ 0 \\ 0 \end{pmatrix} + P \begin{pmatrix} 1 \\ \cos 2\beta \cos 2\chi \\ \cos 2\beta \sin 2\chi \\ \sin 2\beta \end{pmatrix} \right\} \tag{2.24}$$

2.3.2 PHOTOELECTRIC EFFECT

The photoelectric effect is an indirect photon–photon process. In the photoelectric effect a photon is absorbed by an atom creating a hole in the atom with the ejection of an electron. The energy of this electron is the difference between that of the incident photon and of the binding energy of the electron. The vacancy will be spontaneously filled by an electron transition from a higher energy level (Figure 2.4). The de-excitation energy is carried off with the emission of a characteristic photon or Auger electrons. Statistically, the two combined processes (absorption–ejection) may be considered as a single interaction. The theory of the photoionization process has received considerable attention [15–17]. The photoelectric cross-section has been investigated with experiments and theoretical calculations [18], and collected data are available in the literature [19,8].

The scalar kernel for the production of a characteristic line of wavelength λ [20] from a pure element target due to the photoelectric absorption of photons with wavelength λ' is given by [21]

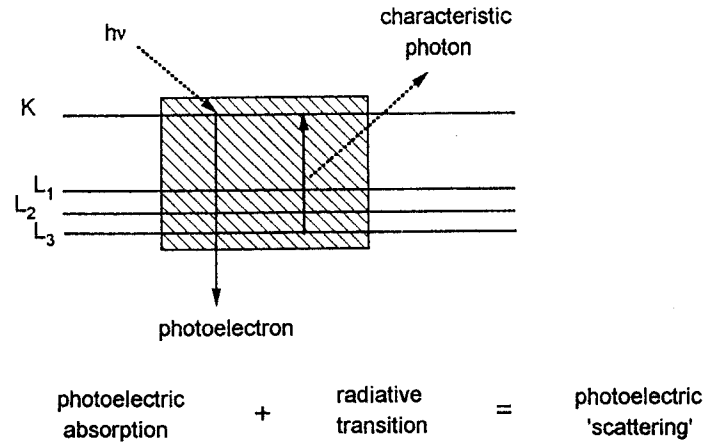

Figure 2.4 A photoelectric absorption followed by a radiative transition to the created vacancy can be considered as photoelectric scattering, giving one characteristic photon and one photoelectron, because of the short time interval between these two processes.

$$k_{P_{\lambda_i}}(\vec{\omega}, \lambda, \vec{\omega}', \lambda') = \frac{1}{4\pi} Q_{\lambda_i}(\lambda') \delta(\lambda - \lambda_i)[1 - \cup(\lambda' - \lambda_{e_i})] \tag{2.25}$$

The isotropy of the secondary X-rays is reflected by the kernel independence on $\vec{\omega}$ and by the $(4\pi)^{-1}$ normalization factor. The line is assumed to be monochromatic, neglecting its natural width [22] which is significantly less than the instrumental width [23]. The XRF emission probability density $Q_{\lambda_i}(\lambda')$ for a line λ_i which belongs to a series, is given (in cm^{-1}) by the relationship

$$Q_{\lambda_i}(\lambda') = \tau_s(\lambda') g_{e_i} \Gamma_{\lambda_i} \tag{2.26}$$

where g_{e_i} denotes the radiative fraction for the given series of transitions. The fraction of vacancies g_K, produced in the K subshell, will be filled with transitions from other higher shells giving

$$g_K = (1 - 1/J_K)\omega_K \tag{2.27}$$

The allowed transitions to a subshell can be either radiative or radiationless. Radiative transitions clearly lead to a characteristic line emission. However, radiationless transitions can be of two types, Auger and Coster–Krönig. The Auger effect is produced when the X-ray photon originated in the transition is absorbed by an outer electron of the atom, which is subsequently ejected. Therefore, the Auger electron ejection produces a doubly ionized atom, without photon emission. Coster–Krönig transitions produce transitions within subshells of the same shell. This makes it possible for a given subshell to receive contributions coming from different higher subshells, to produce the same group of lines. For instance, the probabilities for the emission of L_1, L_2 or L_3 lines are given by

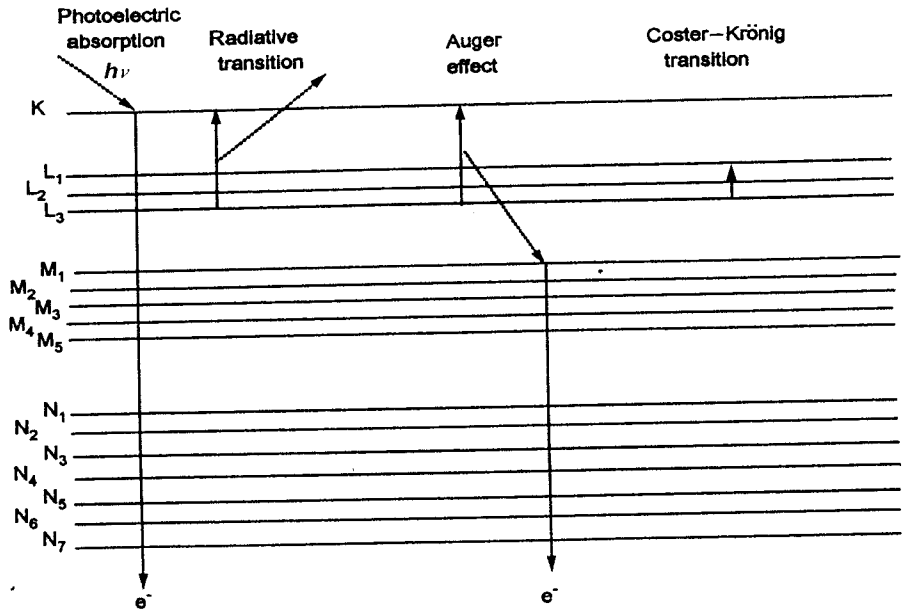

Figure 2.5 Diagram comparing Auger and Coster–Krönig transitions with radiative transitions.

$$g_{L_1} = (1 - 1/J_{L_1})\omega_{L_1} \tag{2.28}$$

$$g_{L_2} = [(1 - 1/J_{L_2}) + f_{12}(1 - 1/J_{L_1})\omega_{L_2} \tag{2.29}$$

$$g_{L_3} = [(1 - 1/J_{L_3}) + f_{23}(1 - 1/J_{L_2}) + (f_{13} + f_{12}f_{23})(1 - 1/J_{L_1})\omega_{L_3} \tag{2.30}$$

where f_{12}, f_{13} and f_{23} are, respectively, the probabilities for the ocurrence of the Coster–Krönig radiationless transitions $L_1 \rightarrow L_2, L_1 \rightarrow L_3$ and $L_2 \rightarrow L_3$ (Figure 2.5) [24–34].

In Eqn (2.26), $\tau_s(\lambda')$ represents the photoelectric attenuation coefficient (cm^{-1}) of the emitter element s for the corresponding subshell, J_{e_i} represents the absorption-edge jump [4, 8, 9, 19], ω_{e_i} the fluorescence yield of the subshell, and Γ_{λ_i} the line emission probability of the line at λ_i into its own spectral series [35–39]. Compilations of calculated values of $\tau_s(\lambda')$ for neutral atoms with a relativistic Hartree–Slater model are available, renormalized to the Hartree–Fock model for $Z = 2 - 54$ [40–42], and without renormalization [8, 9, 43]. A discussion about the significance of normalization is given by Saloman and Hubbell [44]. The line is emitted only when λ' is lower than the threshold of the absorption edge wavelength λ_{e_i} of the series to which the line belongs [9, 45], as represented by the Heaviside function $\cup$ in equation (2.25) (Figure 2.6).

The complete emission spectrum of the element s is obtained by adding all the single lines emitted by absorption of radiation of wavelength λ':

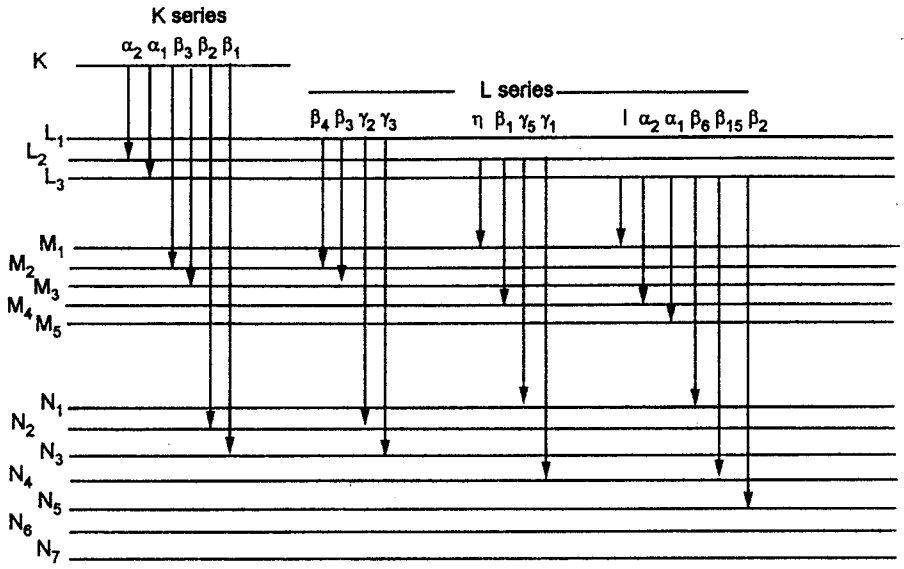

Figure 2.6 Nomenclature of X-ray transitions.

$$k_P(\vec{\omega}, \lambda, \vec{\omega}', \lambda') = \frac{1}{4\pi} \sum_i Q_{\lambda_i}(\lambda')\delta(\lambda - \lambda_i)[1 - \cup(\lambda' - \lambda_{e_i})] \tag{2.31}$$

It is worth noting that the integral (2.10) of the kernel defined by Eqn (2.31) cannot yield the photoelectric coefficient τ. The reason is that the attenuation coefficient is formed by both an absorption part and a scattering part (the scattering here is represented by the spontaneous emission of characteristic photons). The emission does not compensate the absorption exactly, because every absorbed photon does not produce a characteristic photon. Therefore, an integral over all the characteristic photons cannot return the number of the absorbed ones.

Matrix version of the photoelectric kernel for the vector equation

The photoelectric effect has low sensitivity to the polarization state of the incident photon but is not completely insensitive to it. According to Flügge *et al.* [46], after photoionization, the fluorescence X-rays originating from the vacancy states with $j = 1/2$, (K shell and L_1, L_2, M_1 and M_2 subshells, etc.) will only be isotropic and unpolarized. However those fluorescence X-rays that are emitted from the filling of vacancy states with $j = 3/2$ (L_3, M_3 and M_4 subshells) and with $j = 5/2$, (M_5 subshell) will be anisotropic and polarized. This theoretical prediction was recently confirmed experimentally by Kahlon *et al.* [47] supporting the hypothesis that the vacancy states with $j > 1/2$ have a

non-statistical population distribution of their magnetic substates and are aligned. The level of percentage polarization measured by these authors for the L_l and L_α lines was 86(6)% and 29(2)% for Th, and 79(6)% and 36(2)% for U. However, recent measurements on the L_3 subshell X-ray lines of erbium by Papp and Campbell [48] reveal a considerably less consistent anisotropy than that reported by Kahlon *et al.* [47], and estimate the anisotropy for the L_α doublet (containing about the 80% of the L_3 X-rays) to be less than 2%. It is worth noting that this controversy does not affect the existence of the non-statistical population distribution mentioned above, but only the extent of the anisotropy that in the last case could be practically negligible.

Assuming that photoelectric X-ray emission is independent of polarization, we can write the matrix kernel for the emission of a characteristic line of wavelength λ_i as

$$\mathbf{K}^{(S)}_{P_{\lambda_i}}(\vec{\omega},\lambda,\vec{\omega}',\lambda') = k_{P_{\lambda_i}}(\vec{\omega},\lambda,\vec{\omega}',\lambda')\begin{pmatrix}1&0&0&0\\0&0&0&0\\0&0&0&0\\0&0&0&0\end{pmatrix} \tag{2.32}$$

where the scalar kernel was defined in equation (2.25). The complete emission spectrum can be obtained similarly as in equation (2.31).

2.3.3 RAYLEIGH SCATTERING

Coherent scattering is a process where photons change direction (momentum transfer) but not energy [11]. This scattering takes place with the more tightly bound electrons of the atom which behave rigidly during the interaction. In a first approximation the coherent scattering by a free electron was studied by J. J. Thomson using classical electrodynamics [3]:

$$\left(\frac{\mathrm{d}\sigma}{\mathrm{d}\omega\mathrm{d}\lambda}\right)_{\text{Thomson}} = \frac{r_e^2}{2}(1+(\vec{\omega}\cdot.\vec{\omega}')^2)\delta(\lambda-\lambda') \tag{2.33}$$

where r_e is the classical radius of the electron. The delta function stresses the monochromaticity of the scattering. In many electron atoms, a cooperative effect is verified by the scattering from all the electrons in the atom (Rayleigh scattering). As the scattering is coherent, the amplitudes must be added before squaring to obtain the intensity. Therefore, the cross-sections for electron results are non-additive, and we have to define an atomic differential cross-section as

$$\begin{aligned}\left(\frac{\mathrm{d}^2\sigma_R}{\mathrm{d}\lambda\mathrm{d}\omega}\right)_{at} &= F^2(\lambda',\vec{\omega}\cdot\vec{\omega}',Z)\left(\frac{\mathrm{d}^2\sigma}{\mathrm{d}\lambda\mathrm{d}\omega}\right)_{\text{Thomson}} \\ &= \frac{r_e^2}{2}(1+(\vec{\omega}\cdot\vec{\omega}')^2)F^2(\lambda',\vec{\omega}\cdot\vec{\omega}',Z)\delta(\lambda-\lambda')\end{aligned} \tag{2.34}$$

The square form factor $F^2(\lambda',\vec{\omega}\cdot\vec{\omega}',Z)$ produces atomic contributions significantly greater than Z times the contribution from one single electron. In terms of the transferred momentum $\vec{q}$, the form factor for an atom of Z electrons has been defined as the matrix element [49]:

$$F(\vec{q},Z) = \sum_{n=1}^{Z}\langle\Psi_0|\exp(i\vec{q}\cdot\vec{r}_n)|\Psi_0\rangle \tag{2.35}$$

where $\vec{r}_n$ denotes the instantaneous position of the nth electron and Ψ_0 the ground-state wavefunction. Hubbell et al. reviewed exhaustively the computation of the form factor [50]. By defining the transferred momentum as

$$x = \lambda[\text{Å}]^{-1}\sin\left(\frac{\Theta}{2}\right) \tag{2.36}$$

for given wavelength and scattering angle Θ they computed tables of $F(x,Z)$ for all the elements in the periodic table. Experimental data and other tables may be found in more recent works by Hubbell and Øverbø [51], Schaupp *et al.* [52] and Kane *et al.* [11]. Some special limits of the form factor are $F(0,Z) = Z$ and $F(\infty,Z) = 0$. The Rayleigh atomic kernel for unpolarized photons, with phase-space coordinates $(\vec{\omega}',\lambda')$ scattered by a pure element target of atomic number Z into the coordinates $(\vec{\omega},\vec{\lambda})$, is defined as

$$\begin{aligned}k_R(\vec{\omega},\lambda,\vec{\omega}',\lambda') &= \frac{\rho N}{A}\left(\frac{\mathrm{d}^2\sigma_R}{\mathrm{d}\lambda\mathrm{d}\omega}\right)_{at} \\ &= \sigma\delta(\lambda-\lambda')\left(1+(\vec{\omega}\cdot\vec{\omega}')^2\right)F^2(\lambda',\vec{\omega}\cdot\vec{\omega}',Z)\end{aligned} \tag{2.37}$$

where $\sigma = \rho N r_e^2/(2A)$ is a macroscopic attenuation coefficient (in cm^{-1}). The angular dependence of the kernel (2.37) is due to the last two factors: the Thomson angular factor representing an average polarization state, and the square of the atomic form factor comprising the constructive interference from the whole charge distribution.

A closed approximate expression for F was given by Veigele *et al.* using the Thomas–Fermi model [53]:

$$F(\mathbf{U}) = Z\left[(1+\exp(-0.3))\exp\left(-1.49\mathbf{U}^{0.388}\right)+0.00327\right] \tag{2.38}$$

with

$$\mathbf{U} = 2\frac{137\lambda_c}{Z^{\frac{1}{3}}\lambda}\sin\frac{\Theta}{2} \tag{2.39}$$

More precise values are achieved with semi-empirical formulae and fitting coefficients of theoretical calculations [54, 55], or interpolating values in Hubbell's tables in the ENDF-6 data file [9, 56]. Cullen has developed a fitting tool to compute fitting coefficients for user-defined fitting functions of different complexities for the form factor, using the ENDF-6 file [57]. The integration of

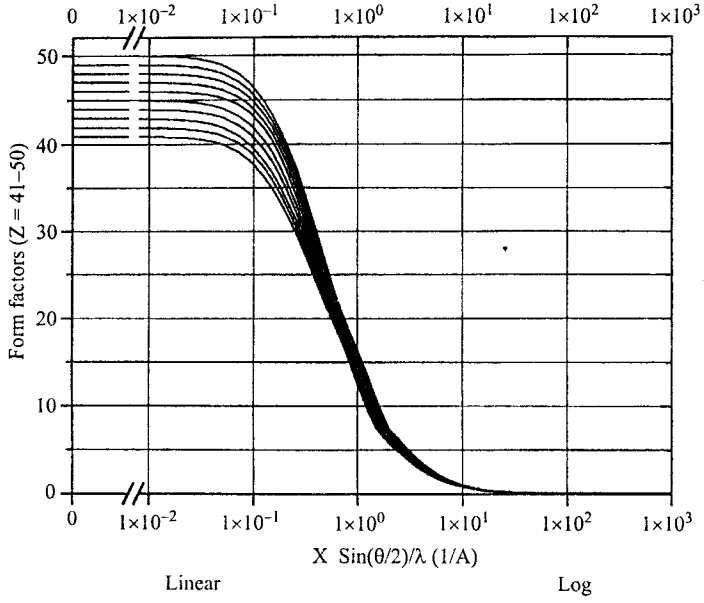

Figure 2.7 Plots of form factors for several elements. Data taken from Ref. 55.

the scalar kernel (2.37) giving the total Rayleigh coefficient can be used for checking the form factor data consistency. Values for the integrals are available, either from numerical integration [4, 50], or from the analytical integration of the approximated form factor [58] (Figure 2.7).

Matrix version of the Rayleigh kernel for the vector equation

Assuming that electron binding (in many-electron atoms) can be described by a polarization independent form factor [11, 59, 60], the matrix kernel for Rayleigh scattering of polarized radiation becomes

$$\mathbf{K}_{\mathrm{R}}^{(\mathrm{S})}(\vec{\omega},\lambda,\vec{\omega}',\lambda') = \frac{k_{\mathrm{R}}(\vec{\omega},\lambda,\vec{\omega}',\lambda')}{1+(\vec{\omega}\cdot\vec{\omega}')^2}\begin{pmatrix} (\vec{\omega}\cdot\vec{\omega}')^2+1 & (\vec{\omega}\cdot\vec{\omega}')^2-1 & 0 & 0 \\ (\vec{\omega}\cdot\vec{\omega}')^2-1 & (\vec{\omega}\cdot\vec{\omega}')^2+1 & 0 & 0 \\ 0 & 0 & 2\vec{\omega}\cdot\vec{\omega}' & 0 \\ 0 & 0 & 0 & 2\vec{\omega}\cdot\vec{\omega}' \end{pmatrix} \tag{2.40}$$

2.3.4 COMPTON SCATTERING

In the case of incoherent scattering, energy as well as direction is changed [61, 62]. This process takes place with the outer electrons of the atom. In a first approximation the Compton effect can be studied by considering the collision of one photon carrying energy $h\nu'$, momentum $p' = h\nu'/c$ and traveling with

direction $\vec{\omega}'$, against a free electron at rest (mass rest energy $m_e c^2$, null momentum). Conservation of energy and momentum during the hit establishes that, if the photon scatters with a scattering angle Θ, it carries a wavelength $\lambda = \lambda' + \lambda_C(1-\cos\Theta)$. Here $\cos\Theta = \vec{\omega}'\cdot\vec{\omega}$, and $\lambda_C = h/m_e c = 0.024\,263\,1$ Å is the Compton wavelength. The validity of this approximation is considered as a proof of the particle nature of the photon. In agreement with the approximation, scattering experiments for a narrowly defined scattering angle show a well defined peak at a wavelength higher than the incident one. The differential electronic cross-section for the described collision (average polarization) has been computed [63, 64] as

$$\left(\frac{\mathrm{d}\sigma}{\mathrm{d}\omega\mathrm{d}\lambda}\right)_e = \frac{r_e^2}{2}K_{\mathrm{KN}}(\lambda,\lambda')\frac{1}{\lambda_C}\delta\left(1-\vec{\omega}\cdot\vec{\omega}'+\frac{\lambda-\lambda'}{\lambda_C}\right) \tag{2.41}$$

where

$$K_{\mathrm{KN}}(\lambda,\lambda') = \left(\frac{\lambda'}{\lambda}\right)^2\left\{\frac{\lambda}{\lambda'}+\frac{\lambda'}{\lambda}+\frac{\lambda-\lambda'}{\lambda_C}\left(\frac{\lambda-\lambda'}{\lambda_C}-2\right)\right\} = \left(\frac{\lambda'}{\lambda}\right)^2\left\{\frac{\lambda}{\lambda'}+\frac{\lambda'}{\lambda}-\sin^2\Theta\right\} \tag{2.42}$$

The direction–wavelength delta in equation (2.41) fixes the integration path in the phase-space along the line $1-\vec{\omega}\cdot\vec{\omega}'+(\lambda'-\lambda)/\lambda_C = 0$ (this condition does not account for the shift for bound electrons [62]).

Compton kernel in the Waller–Hartree approximation

When the energy of the exciting photons is comparable with the binding energy of the inner-shell electrons of the target, a departure from the Klein–Nishina cross-section is verified. It is customary to define the Waller–Hartree incoherent scattering function $S^{\mathrm{WH}}(\vec{q},Z)$ which takes into account the electron binding for the whole atom [65] as

$$S^{\mathrm{WH}}(\vec{q},Z) = \sum_{m=1}^{Z}\sum_{n=1}^{Z}\langle\Psi_0|\exp(i\vec{q}\cdot(\vec{r}_m-\vec{r}_n))|\Psi_0\rangle - \left|\sum_{m=1}^{Z}\langle\Psi_0|\exp(i\vec{q}\cdot\vec{r}_m)|\Psi_0\rangle\right|^2 \tag{2.43}$$

where $\vec{q}$ denotes the transferred momentum during the collision, $\vec{r}_m$ and $\vec{r}_n$ are the instantaneous positions of the mth and nth electrons, respectively, and Ψ_0 is the ground-state wavefunction. Hubbell *et al.* reviewed exhaustively the computational techniques for obtaining the scattering function [50]. By defining the transferred momentum as in Eqn (2.36), they computed tables of $S^{\mathrm{WH}}(x,Z)$ for all the elements in the periodic table. Special limits of the scattering function are $S^{\mathrm{WH}}(0,Z) = 0$ and $S^{\mathrm{WH}}(\infty,Z) = Z$. The double differential atomic cross-section for incident photons, with phase-space coordinates $(\vec{\omega}',\lambda')$ scattered by a pure specie target of atomic number Z into the coordinates $(\vec{\omega},\lambda)$, is expressed as

$$\left(\frac{\mathrm{d}^2\sigma}{\mathrm{d}\lambda\mathrm{d}\omega}\right)_{\mathrm{at}}^{\mathrm{WH}} = \frac{r_e^2}{2}K_{\mathrm{KN}}(\lambda,\lambda')S^{\mathrm{WH}}(x,Z)\frac{1}{\lambda_C}\delta\left(1-\vec{\omega}\cdot\vec{\omega}'+\frac{\lambda-\lambda'}{\lambda_C}\right) \tag{2.44}$$

Therefore, the Compton kernel is

$$k_{(C)}^{\mathrm{WH}}(\vec{\omega},\lambda,\vec{\omega}',\lambda') = \frac{\rho N}{A}\left(\frac{\mathrm{d}^2\sigma}{\mathrm{d}\lambda\mathrm{d}\omega}\right)_{\mathrm{at}}^{\mathrm{WH}} = \sigma K_{\mathrm{KN}}(\lambda,\lambda')S^{\mathrm{WH}}(x,Z)\frac{1}{\lambda_{\mathrm{C}}}\delta\left(1-\vec{\omega}\cdot\vec{\omega}'+\frac{\lambda-\lambda'}{\lambda_{\mathrm{C}}}\right) \tag{2.45}$$

An approximated formula for S^{WH} was obtained with the Thomas–Fermi model derived by Veigele *et al.* [53]:

$$S^{\mathrm{WH}}(\mathrm{V}) = Z\lfloor 1-\exp(-4.88\mathrm{V}^{0.856})\rfloor \tag{2.46}$$

with

$$\mathrm{V} = \frac{2}{3}\frac{137\lambda_{\mathrm{C}}}{Z^{\frac{1}{3}}\lambda}\sin\frac{\Theta}{2} \tag{2.47}$$

More precise values of $S^{\mathrm{WH}}(x,Z)$ can be computed using semi-empirical formulas and fitting coefficients to theoretical calculations [66], or interpolating values in the Hubbell's tables in the ENDF-6 data file [9, 56]. Cullen has developed a tool to compute fitting coefficients for user-defined functions of different complexities for the scattering function, using the ENDF-6 file [57] (Figure 2.8).

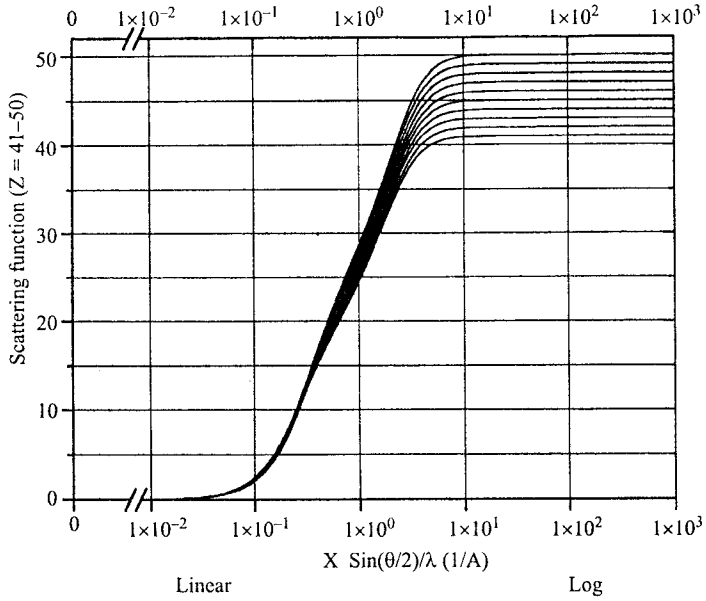

Figure 2.8 Plots of scattering functions for several elements. Data taken from Ref. 66.

Compton kernel in the impulse approximation

In the previous section the precollision motion of the electrons has been ignored in the kernel equation (2.45), limiting the Compton peak to a monochromatic line. Because of the Compton profile (that is the projection of the electron momentum distribution on the z axis) the width of the scattered peak is larger than the instrumental width [67]. The more rigorous theoretical treatment associated with the Compton profile is discussed in this section.

If we define as $p_z = \vec{p}\cdot\vec{q}/q$ the projection of the momentum of the interacting electron on the scattering vector $\vec{q} = \vec{k} - \vec{k}'$ (where $\vec{k}'$ and $\vec{k}$ are the momenta of the incident and scattered photons), then it can be demonstrated that the Compton shift produced by a moving electron is also a function of p_z:

$$\lambda = \lambda' + \lambda_{\mathrm{C}}(1-\vec{\omega}\cdot\vec{\omega}') - \frac{p_z}{mc}(\lambda'^2+\lambda^2-2\lambda\lambda'\vec{\omega}\cdot\vec{\omega}')^{1/2} \tag{2.48}$$

It is customary to use the dimensionless variable Q defined as [68]

$$\frac{p_z}{mc} = \frac{e^2}{4\pi\varepsilon_0 hc}Q \approx \frac{Q}{137} \tag{2.49}$$

in place of p_z in Eqn (2.48). However, a bound electron in the atom does not hold a definite state of momentum as shown in Eqn (2.48), but has a momentum distribution that depends on the subshell occupied by the electron. If we denote with an index i the subshell occupied by the electron, the Compton profile is related to the momentum distribution $\rho(p)$ of the scatterer before the collision through the relationship

$$J_i(Q) = \frac{1}{2}\int_{\mathrm{Q}}^{\infty}\rho(p)p\mathrm{d}p \tag{2.50}$$

As a consequence of wavefunction normalization, the integrated profile must satisfy the condition

$$2\int_0^{\infty} J_i(Q)\mathrm{d}Q = 1 \tag{2.51}$$

To deduce the Compton intensity in the impulse approximation (IA) we use the relationships.

$$\left(\frac{d\sigma}{\mathrm{d}\omega}\right)_{\mathrm{at}} = \int_0^{\infty}\left(\frac{\mathrm{d}^2\sigma}{\mathrm{d}\lambda\mathrm{d}\omega}\right)_{\mathrm{at}}\mathrm{d}\lambda \tag{2.52}$$

and

$$\left(\frac{d\sigma}{\mathrm{d}\omega}\right)_{\mathrm{at}}^{\mathrm{WH}} \cong \left(\frac{\mathrm{d}\sigma}{\mathrm{d}\omega}\right)_{\mathrm{at}}^{\mathrm{IA}} \tag{2.53}$$

implying that the scattering function should be equivalent in both representations [13]:

$$S^{WH} \cong S^{IA} \tag{2.54}$$

From Eqns (2.45), and (2.52)–(54) we obtain

$$\frac{\rho N}{A}\left(\frac{d\sigma}{d\omega}\right)_{at}^{WH} = \sigma K_{KN}(\lambda_p, \lambda') S^{WH}\left(\frac{1}{\lambda'}\sqrt{\frac{1-\vec{\omega}\cdot\vec{\omega}'}{2}}, Z\right)$$
$$\cong \sigma K_{KN}(\lambda_p, \lambda') S^{IA}(\lambda', \vec{\omega}\cdot\vec{\omega}', Z) \tag{2.55}$$

where $\lambda_p = \lambda' + \lambda_C(1 - \vec{\omega}\cdot\vec{\omega}')$ is the peak wavelength. As the scattering function for the atom in the impulse approximation is obtained as a sum of the contributions from all the subshells, we have

$$S^{IA}(\lambda', \vec{\omega}\cdot\vec{\omega}', Z) = \sum_{i}^{OCC} \int_{-\infty}^{Q_{i,max}} J_i(Q) dQ \tag{2.56}$$

where $Q_{i,max}$ is obtained by putting $\lambda = hc/E = hc/(E' - I_i)$ (I_i being the binding energy of the subshell) in the expression

$$Q = \frac{137[\lambda' + \lambda_C(1 - \vec{\omega}\cdot\vec{\omega}') - \lambda]}{(\lambda'^2 + \lambda^2 - 2\lambda\lambda'\vec{\omega}\cdot\vec{\omega}')^{1/2}} \tag{2.57}$$

which is obtained straightforwardly from Eqn (2.48). The integral in Eqn (2.56) represents the contribution of one electron in the subshell i to the scattering function. Being a contribution that is upper limited by $Q_{i,max}$, it is equivalent to integrating with a higher upper limit the subshell profile truncated at $Q_{i,max}$, i.e.

$$\int_{-\infty}^{Q_{i,max}} J_i(Q) dQ = \int_{-\infty}^{\infty} J_i(Q, Q_{i,max} dQ \tag{2.58}$$

The sum over the occupied states in the right-hand side of Eqn (2.56) can be shifted into the integral. In this way we can define the whole profile at $\lambda', \vec{\omega}\cdot\vec{\omega}'$ and Z as the overlap of the truncated profiles of the Z electrons of the element (Figure 2.9), i.e.

$$J(Q, \lambda', \vec{\omega}\cdot\vec{\omega}', Z) = \sum_{i}^{OCC} J_i(Q, Q_{i,max}) \tag{2.59}$$

Equation (2.56) can be rewritten by making a change of variable in the integral:

$$S^{IA}(\lambda', \vec{\omega}\cdot\vec{\omega}', Z) = \int_0^{\infty} J(Q(\lambda), \lambda', \vec{\omega}\cdot\vec{\omega}', Z)\frac{dQ}{d\lambda} d\lambda \tag{2.60}$$

From Eqns (2.48), (2.55) and (2.60) we can write the IA equivalent of Eqn (2.45) as

$$k_C^{IA}(\lambda, \vec{\omega}, \lambda', \vec{\omega}') = \frac{\rho N}{A}\left(\frac{d\sigma}{d\lambda d\omega}\right)_{at}^{IA}$$
$$\cong \sigma K_{KN}(\lambda_p, \lambda') J(Q(\lambda), \lambda', \vec{\omega}\cdot\vec{\omega}', Z)\frac{dQ}{d\lambda} \tag{2.61}$$

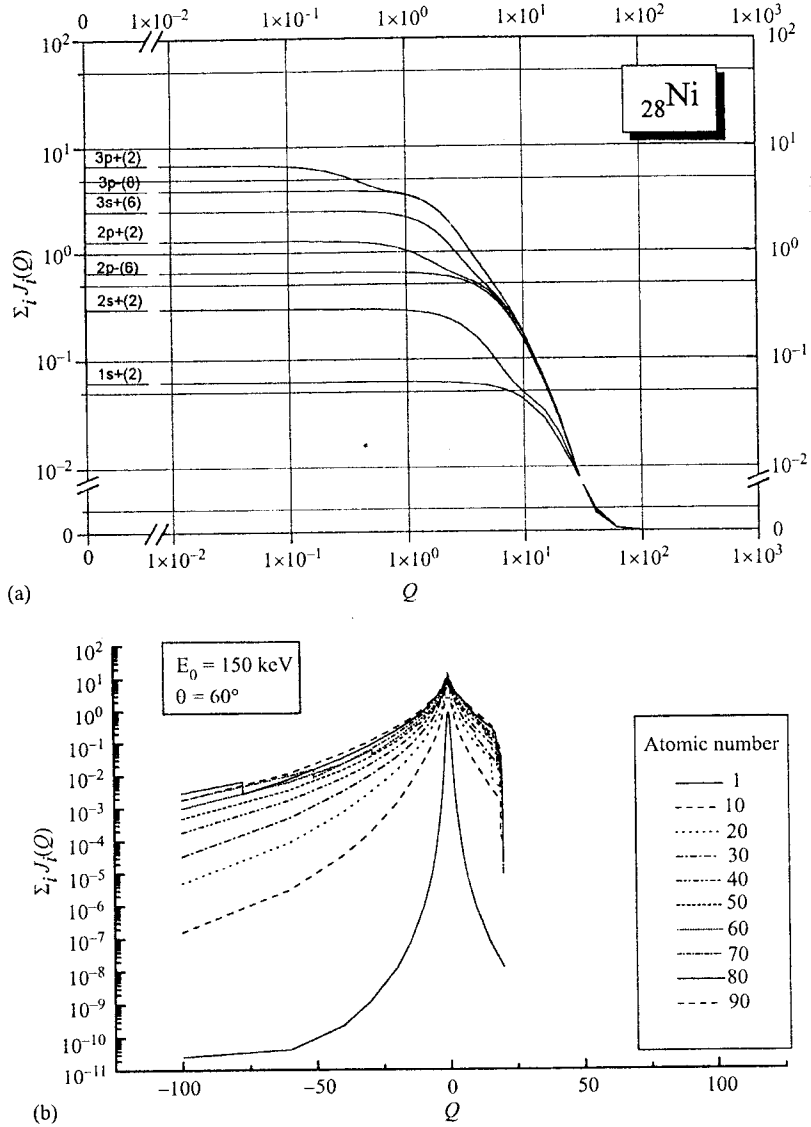

Figure 2.9 (a) Contributions of the configuration electrons to the Compton profile of Ni; (b) Compton profiles for several elements. The excitation energy is 150 keV, and the scattering angle is 60°. Data taken from Ref. 68.

where

$$\frac{dQ}{d\lambda} = -137(1 - \vec{\omega}\cdot\vec{\omega}')\frac{[\lambda'(\lambda' - \lambda_C\vec{\omega}\cdot\vec{\omega}') + \lambda(\lambda' + \lambda_C)]}{(\lambda'^2 + \lambda^2 - 2\lambda\lambda'\vec{\omega}\cdot\vec{\omega}')^{1/2}} \tag{2.62}$$

is obtained from Eqn (2.57). Equation (2.61) represents the alternative to Eqn (2.45) using Compton profiles. As the broadening of the Compton peak is considerable, the IA gives a much more precise estimate of the intensity distribution of the Compton peak, especially with respect to spectrum build-up in the X-ray regime.

Matrix version of the Compton kernel for the vector equation

A Klein–Nishina coefficient for linear polarization could be written in place of the coefficient defined in Eqn (2.42), which depends on the angle between the directions of the electric vectors of the incident ($\vec{\varepsilon}'$) and scattered ($\vec{\varepsilon}$) beams [62, 63, 69]. It shows the familiar relationship

$$K_{\mathrm{KN}}^{\mathrm{tp}}(\lambda,\lambda') = \left(\frac{\lambda'}{\lambda}\right)^2 \left\{\frac{\lambda}{\lambda'} + \frac{\lambda'}{\lambda} - 2 + 4(\vec{\varepsilon}\cdot\vec{\varepsilon}')^2\right\} \tag{2.63}$$

The above statement means that the scattering cross-section determines the probability for a plane polarized photon to be scattered in a certain direction and then pass through a hypothetical filter which accepts only radiation polarized in a certain plane. Elliptical polarization is not considered by such a treatment. Therefore, for a complete analysis of the polarization effects, it is more convenient to use the Stokes' representation.

Assuming that the effect of charge distribution (in many-electron atoms) contributes a polarization independent scattering function and the spin of the electron is randomly oriented before, and is not observed after the scattering [70], the matrix kernel for Compton scattering becomes

$$\mathbf{K}_{\mathrm{C}}^{(\mathrm{S})}(\vec{\omega},\lambda,\vec{\omega}',\lambda') = \frac{k_C(\vec{\omega},\lambda,\vec{\omega}',\lambda')}{a+b(b-2)} \begin{pmatrix} a+b(b-2) & b(b-2) & 0 & 0 \\ b(b-2) & 2+b(b-2) & 0 & 0 \\ 0 & 0 & 2(1-b) & 0 \\ 0 & 0 & 0 & a(1-b) \end{pmatrix} \tag{2.64}$$

where the dimensionless variables are

$$a = \frac{\lambda}{\lambda'} + \frac{\lambda'}{\lambda}; b = \frac{\lambda-\lambda'}{\lambda_C}$$

In the limiting case of $\lambda = \lambda' \to \infty$, we obtain the matrix of Rayleigh scattering.

For studying the effects of non-linear polarization on the scattering of X-rays in a target exposed to a magnetic field it is useful to consider a more complete kernel including the magnetic terms omitted in equation (2.64). This matrix kernel can be obtained to a first approximation by considering Compton scattering by a free electron exposed to an external magnetic field, and becomes [71]

$$\mathbf{K}_{\mathrm{C}}^{(\mathrm{S})}(\vec{\omega},\lambda,\vec{\omega}',\lambda) = \frac{r_0^2}{2\lambda_C}\left(\frac{\lambda'}{\lambda}\right)^2 \delta\left(1-\vec{\omega}\cdot\vec{\omega}'+\frac{\lambda'-\lambda}{\lambda_C}\right)$$
$$\begin{pmatrix} a+b(b-2) & b(b-2) & 0 & b((1-b)c'\vec{n}'+c\vec{n})\cdot\vec{S} \\ b(b-2) & 2+b(b-2) & 0 & bc'\vec{n}\times\vec{n}\cdot\vec{n}'\times\vec{S} \\ 0 & 0 & 2(1-b) & bc\vec{n}\times\vec{n}'\cdot\vec{S} \\ b((1-b)c\vec{n}+c'\vec{n}')\cdot\vec{S} & bc'\vec{n}'\times\vec{n}\cdot\vec{n}\times\vec{S} & bc'\vec{n}'\times\vec{n}\cdot\vec{S} & a(1-b) \end{pmatrix} \tag{2.65}$$

where $c = \lambda_C/\lambda$ and $c' = \lambda_C/\lambda'$ are auxiliary variables, $\vec{n} = \vec{k}/k$ and $\vec{n}' = \vec{k}'/k'$ are the directions of the scattered and incident photons, and $\vec{S}$ is the spin orientation of the electron before the scattering. It is apparent that some new non-zero terms appear in the last row and column of the matrix. They are due to a specific rather than an average orientation for the spin of the electron. These terms introduce coupling for the last Stokes' component of the flux, responsible of the ellipticity, i.e. of the non-linearity of the polarization state. It is this coupling that avoids consideration of the transport equation corresponding to the V component as a separate, uncoupled equation, as for the case of linear polarization.

Several authors have paid attention to the build-up of a much more detailed description of the differential cross-section, depending on the initial and final polarization states of both the interacting photon and electron [71–78] but this extent of detail is excessive for the scope of this chapter.

In order to extend the kernel (2.65) to atoms with many electrons [79, 80], we must consider the distribution of the magnetization in addition to that of the electric charge. Therefore, the matrix kernel becomes more complex than the kernel (2.64) that was obtained in absence of the magnetic field. This means that the complete matrix kernel is the sum of two matrix terms, one dependent on the electric charge distribution, as in Eqn (2.64), and the other dependent on the magnetization distribution. For the last distribution it is convenient to define a magnetic form factor which, in analogy to the charge form factor, can be expressed [81, 82] as the modulus of the spatial Fourier transform of the spin density:

$$F^{\mathrm{M}}(\vec{q}) = \left|\sum_{j=1}^{Z} \vec{s}_j e^{i\vec{q}\cdot\vec{r}_j}\right| = \frac{1}{2\mu_B}\left|\int d^3r e^{i\vec{q}\cdot\vec{r}}\vec{M}_{\mathrm{S}}(\vec{r})\right| \tag{2.66}$$

where $\vec{s}_j$ and $\vec{r}_j$ are the spin and position of the electron labeled j, $\vec{M}_s(\vec{r})$ is the spin density, μ_B the Bohr magneton, and $\vec{q} = \vec{k} - \vec{k}'$ is the momentum transfer. As the magnetization density is more diffuse spatially than the charge density, the magnetic form factor falls off more rapidly than the charge form factor.

Equation (2.65) does not include the orbital magnetization, which was considered in detail for X-ray diffraction [83–86]. The orbital magnetization should be considered to obtain a formal picture of the magnetic properties of the atom with respect to the polarized radiation. This feature has given rise to

speculation that Compton scattering might be used for separating the magnetization densities of the spin and orbital magnetization [81]. However, more recent studies [87, 88] have found that the orbital magnetization term is negligible at the Compton limit of high-energy photon scattering, whereas it maintains a central importance for Bragg diffraction. For this reason, the orbital magnetization can be omitted to obtain a simplified expression of the complete matrix kernel for the Compton effect:

$$\mathbf{K}_C^{(S)}(\vec{\omega},\lambda,\vec{\omega}',\lambda') = \frac{\sigma}{\lambda_C}\left(\frac{\lambda'}{\lambda}\right)^2 \delta\left(1-\vec{\omega}\cdot\vec{\omega}'+\frac{\lambda'-\lambda}{\lambda_C}\right)$$
$$\left\{ S(\lambda',\vec{\omega}\cdot\vec{\omega}',Z) \begin{pmatrix} a+b(b-2) & b(b-2) & 0 & 0 \\ b(b-2) & 2+b(b-2) & 0 & 0 \\ 0 & 0 & 2(1-b) & 0 \\ 0 & 0 & 0 & a(1-b) \end{pmatrix} \right.$$
$$+F^M(\lambda',\vec{\omega}\cdot\vec{\omega}',Z)$$
$$\left. \begin{pmatrix} 0 & 0 & 0 & b((1-b)c'\vec{n}'+c\vec{n})\cdot\vec{B} \\ 0 & 0 & 0 & bc'\vec{n}\times\vec{n}'\cdot\vec{n}'\times\vec{B} \\ 0 & 0 & 0 & bc\vec{n}\times\vec{n}'\cdot\vec{B} \\ b((1-b)c\vec{n}+c'\vec{n}')\cdot\vec{B} & bc'\vec{n}'\times\vec{n}\cdot\vec{n}\times\vec{B} & bc'\vec{n}'\times\vec{n}\cdot\vec{B} & 0 \end{pmatrix} \right\} \quad (2.67)$$

where $\vec{B}$ is a unitary vector oriented in the direction of the external magnetic field, and $F^M(\lambda',\vec{\omega}\cdot\vec{\omega}',Z)$ is the magnetic form factor expressed as a function of the wavelength and scattering angle instead of the transferred momentum. From Eqn (2.67) it is easy to see that the ratio of the magnetic scattering intensity term related to the usual charge intensity term, is proportional to

$$\frac{F^M(\lambda',\vec{\omega}\cdot\vec{\omega}',Z)\lambda_C}{S(\lambda',\vec{\omega}\cdot\vec{\omega}',Z)\lambda'} \quad (2.68)$$

The factor $\lambda_C/\lambda'(=E'/mc^2)$ is small ($\sim 10^{-2}$) below 50 keV, and this makes the magnetic signal still weaker compared to the electric signal.

2.4 Mathematical description of photon diffusion

The single-process kernels (or probability density functions) defined above for the individual interactions can be used to describe the diffusion of photons into matter, taking into account how collisions during the attenuation process change the phase-space coordinates of the interacting photons. The resulting problem can be formally described in the frame of transport theory by using the Boltzmann equation. There exist different degrees of approximation with which to describe the diffusion of photons. The first and more widely known is the scalar model, which considers a photon that does not modify its (average) polarization state. Under this description, photons behave as neutral particles and the transport description is analogous to that of neutrons. The photon

interactions are described using average polarized differential cross-sections. This approach is customarily used to study the diffusion of unpolarized photons, to a first approximation. A deeper level of detail is reached by including the polarization state of the photon in the transport equation. This is done with recourse to the so-called vector transport equation which describes the transport of photons starting with an arbitrary polarization state. The wave nature of the photon flux is fully represented by the polarization state, whose evolution is described by the vector equation. The vector equation provides a more complete picture of the photon physics during the diffusion process, which allows the treatment of a number of scattering problems closely related to the polarization state of the source.

The flow of X-rays is completely determined in the solution of a transport equation describing the balance between the number of photons of given energy and direction entering and leaving an infinitesimal volume element. This balance may be formulated for conditions where the X-ray source is constant in time (steady-state problem) and, therefore, also the photon flow in the medium.

In what follows we first show the scalar integral–differential Boltzmann transport equation for photons for a simple model of backscattering from an infinitely thick target; second, the vector equation necessary to describe the evolution of the polarization state of the interacting radiation after the collisions is shown; and third, the differences between the two equations is discussed. The selected model assumes that photons only interact in the target, i.e. the photons escaping towards the empty half-space may suffer absorption but cannot be sent back to the target. This model represents fairly well the behavior of radiation in two media of different densities (the density in the sample being much greater than the density in the surrounding empty space or air; Figure 2.10).

2.4.1 SCALAR TRANSPORT EQUATION

The scalar Boltzmann equation for the above model is

$$\eta\frac{\partial}{\partial z}f(z,\vec{\omega},\lambda) = -\mu(\lambda)f(z,\vec{\omega},\lambda) + \int_0^\infty d\lambda' \int_{4\pi} d\omega' \cup(z)k(\vec{\omega},\lambda,\vec{\omega}',\lambda')f(z,\vec{\omega}',\lambda') + I_0\delta(z)\delta(\vec{\omega}-\vec{\omega}_0)\delta(\lambda-\lambda_0) \quad (2.69)$$

where η denotes the directional cosine ω_z, $d\omega' = d\eta' d\varphi'$ is the differential of the solid angle in the direction of the unitary vector $\vec{\omega}'$, and $\cup(z)$ the unitary step Heaviside function. Let us consider a point $\vec{r}$ and an infinitesimal right cylinder with a base area dA centred at $\vec{r}$ and with a height dl, whose lateral surface is parallel to the direction $\vec{\omega}$. We define the flux $f(\vec{r},\vec{\omega},\lambda)d\lambda d\omega$ as the number of

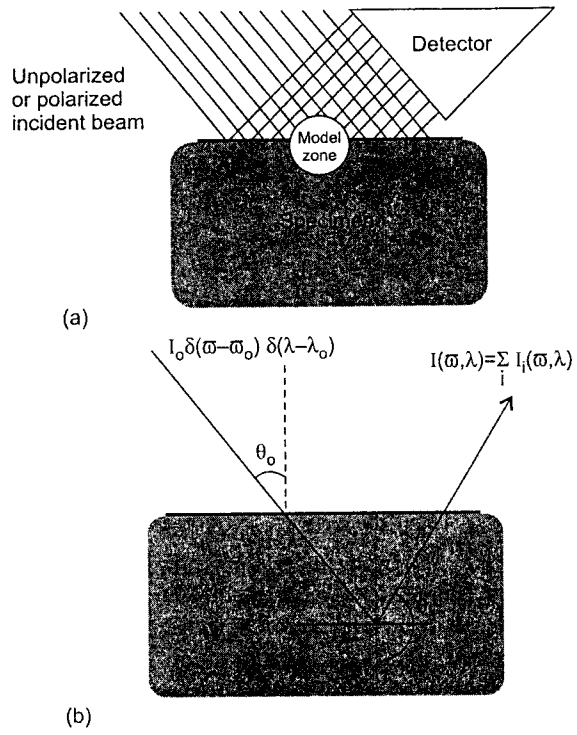

Figure 2.10 Two diagrams for the back-scattering model. (a) Reflection set-up in X-ray spectrometry showing the excitation with a collimated X-ray beam and collimated detection. The circle denotes the zone of applicability of the model. (b) The photon transport equation is solved for a slanted monochromatic beam of unpolarized or polarized X-ray photons.

photons with wavelengths between λ and $\lambda + d\lambda$, and with directions between $\vec{\omega}$ and $\vec{\omega} + d\vec{\omega}$, which cross a unit area of the base of the infinitesimal cylinder per unit time. In Eqn (2.69), $\mu(\lambda)$ is the specimen's total mass attenuation coefficient, $k(\vec{\omega}, \lambda, \vec{\omega}', \lambda')$ is the probability density function of photon scattering into $(\vec{\omega}, \lambda)$ from $(\vec{\omega}', \lambda')$ per unit path through the medium and per unit $d\vec{\omega}$ and $d\lambda$. The term $I_0\delta(z)\delta(\vec{\omega} - \vec{\omega}_0)\delta(\lambda - \lambda_0)$ represents a uniform, plane slant source of intensity I_0 (ph cm^{-2} s^{-1}), producing an incident beam of parallel rays with flight direction $\vec{\omega}_0$ and wavelength λ_0, hitting the infinite sample surface at $z = 0$. It should be noted that, although the scalar transport Eqn (2.69) is one-dimensional in the space coordinates, the flux maintains all the angular information through its dependence on $\vec{\omega}$. According to the model, the empty semi-space in Eqn (2.69) is represented through its non-restitution property, rather than by a change in the density or in the absorption coefficient. This choice allows us to use $\mu(\lambda)$ independent from $\vec{r}$ in the transport equation.

An analytical (orders of interactions) solution for Eqn (2.69) is possible [89], obtained by computing separately the contributions after one, two etc. interactions:

$$f^{(n)}(z,\vec{\omega},\lambda) = \frac{1}{2|\eta|}\int_0^\infty d\tau(1+\operatorname{sgn} z\ \operatorname{sgn}(z-\tau))\exp\left(-\frac{\mu|z-\tau|}{|\eta|}\right) \int_0^\infty d\lambda' \int_{4\pi} d\omega' k(\vec{\omega},\lambda,\vec{\omega}',\lambda') f^{(n-1)}(\tau,\vec{\omega}',\lambda') \tag{2.70}$$

The source term required to start the recursive computation in Eqn (2.70) is given by

$$f^{(0)}(z,\vec{\omega},\lambda) = \frac{I_0}{2|\eta|}\delta(\vec{\omega}-\vec{\omega}_0)\delta(\lambda-\vec{\lambda}_0)(1+\operatorname{sgn}\eta\ \operatorname{sgn} z)\exp\left(-\frac{\mu|z|}{|\eta|}\right) \tag{2.71}$$

Finally, the complete albedo solution for the intensity (i.e. the intensity just on the surface of the sample) can be written as

$$I(\vec{\omega},\lambda) = |\eta| f(0,\vec{\omega},\lambda) = |\eta| \sum_{k=0}^{\infty} f^{(k)}(0,\vec{\omega},\lambda) \tag{2.72}$$

see Figure 2.11.

2.4.2 VECTOR TRANSPORT EQUATION

So far, the scalar Eqn (2.69) has not included rigorously the state of polarization in the description of the radiation field. However, in some cases polarization can be taken into account in the scalar kernels by defining appropriately the interactions between photons and matter. For instance, it is current practice to consider scattering kernels for unpolarized radiation depending on an average state of polarization. This choice gives valid results for the first collision of the incident radiation (assuming a polarization-insensitive detector). However, subsequent collisions have wrong intensities [90] because the equation is not able to describe the polarization acquired or lost through the scattering collisions.

The transport equation describing formally the vector flux $\vec{f}(\vec{r},\vec{\omega},\lambda)d\lambda d\vec{\omega}$ of polarized photons in the Stokes system (having components $f_I(\vec{r},\vec{\omega},\lambda), f_Q(\vec{r},\vec{\omega},\lambda), f_U(\vec{r},\vec{\omega},\lambda)$ and $f_V(\vec{r},\vec{\omega},\lambda)$) for the backscattering framework considered previously can be written as

$$\eta\frac{\partial}{\partial z}\vec{f}^{(s)}(z,\vec{\omega},\lambda) = -\mu(\lambda)\vec{f}^{(s)}(z,\vec{\omega},\lambda) + \int_0^\infty d\lambda' \int_{4\pi} d\vec{\omega}' \cup (z)\mathbf{H}^{(s)}(\vec{\omega},\lambda,\vec{\omega}',\lambda)\vec{f}^{(s)}(z,\vec{\omega}',\lambda') + \delta(z)\vec{S}^{(s)}(\vec{\omega},\lambda) \tag{2.73}$$

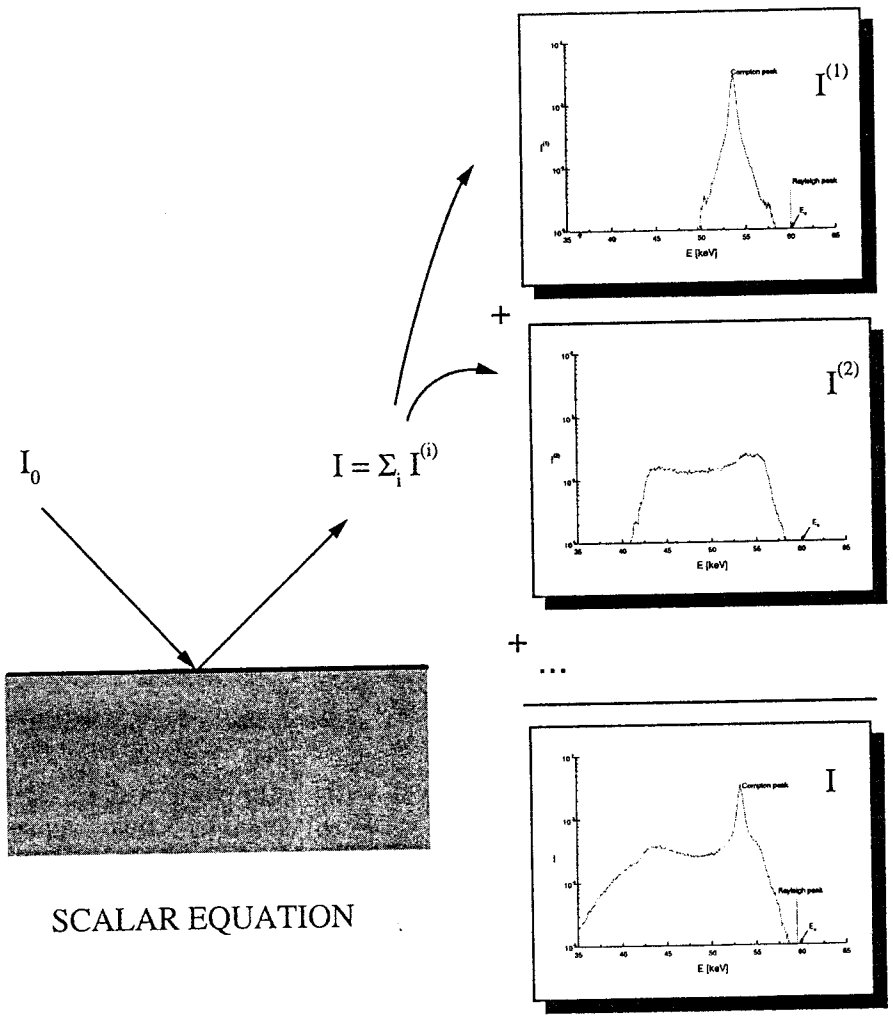

Figure 2.11 Schematic representation of the orders-of-interaction solution obtained with the scalar equation. Each number of collisions contributes a spectral term to the overall spectrum. Every term can be split again into the contributions involving different collision chains of the participating interactions.

where

$$\mathbf{H}^{(s)}(\vec{\omega},\lambda,\vec{\omega}',\lambda') = \mathbf{L}^{(s)}(\pi-\Psi)\mathbf{K}^{(s)}(\vec{\omega},\lambda,\vec{\omega}',\lambda')\mathbf{L}^{(s)}(-\Psi') \tag{2.74}$$

is the kernel matrix in the meridian plane of reference, $\mathbf{K}^{(s)}(\vec{\omega},\lambda,\vec{\omega}',\lambda')$ is the scattering matrix in the scattering plane of reference, and $\mathbf{L}$ is the four-by-four rotation matrix which transforms the scattered flux from the scattering

plane to the meridian plane of the reference. Primed magnitudes denote incidence. The term $\mu(\lambda)$ is the narrow-beam attenuation coefficient which is independent of the state of polarization of the photons (assuming the matter is isotropic), and $\vec{S}^{(s)}(\vec{\omega},\lambda)$ is the source vector flux with components (S_I, S_Q, S_U, S_V). The rotation angles Ψ and Ψ' in Eqn (2.74) are defined by the relationships

$$\cos\Psi = \frac{\eta'\sqrt{1-\eta^2} - \eta\sqrt{1-\eta'^2}\cos(\varphi-\varphi')}{[1-(\vec{\omega}\cdot\vec{\omega}')^2]^{1/2}} \tag{2.75}$$

and

$$\cos\Psi' = \frac{\eta\sqrt{1-\eta'^2} - \eta'\sqrt{1-\eta^2}\cos(\varphi-\varphi')}{[1-(\vec{\omega}\cdot\vec{\omega}')^2]^{1/2}} \tag{2.76}$$

where η and η' are the cosines of the polar angles in spherical geometry, and φ and φ' are the azimuthal angles. For an axis rotation through an angle Φ in the clockwise direction, the matrix $\mathbf{L}$ is defined as

$$\mathbf{L}(\Phi) = \begin{pmatrix} 1 & 0 & 0 & 0 \\ 0 & \cos 2\Phi & \sin 2\Phi & 0 \\ 0 & -\sin 2\Phi & \cos 2\Phi & 0 \\ 0 & 0 & 0 & 1 \end{pmatrix} \tag{2.77}$$

Equation (2.73) represents a system of four integral–differential equations

$$\begin{aligned}\eta\frac{\partial}{\partial z}f_i(z,\vec{\omega},\lambda) = &-\mu(\lambda)f_i(z,\vec{\omega},\lambda) \\ &+\int_0^\infty d\lambda'\int_{4\pi} d\vec{\omega}'\cup(z)\sum_j H_{ij}(\vec{\omega},\lambda,\vec{\omega}',\lambda')f_j(z,\vec{\omega}',\lambda') \\ &+\delta(z)S_i(\vec{\omega},\lambda),(i,j=I,\ Q,\ U,\ V)\end{aligned} \tag{2.78}$$

where H_{ij} denotes the corresponding matrix element of $\mathbf{H}$. It is worth noting that the interaction term introduces coupling between the components of the angular flux as long as $\mathbf{H}$ is non-diagonal.

The solution of the proposed model can be carried out through an orders-of-interaction solution [90],

$$\begin{aligned}f_i^{(n)}(z,\vec{\omega},\lambda) = &\frac{1}{2|\eta|}\int_0^\infty d\tau(1+\operatorname{sgn} z\ \operatorname{sgn}(z-\tau))\exp\left(-\frac{\mu|z-\tau|}{|\eta|}\right) \\ &\int_0^\infty d\lambda'\int_{4\pi} d\omega'\sum_j H_{ij}(\vec{\omega},\lambda,\vec{\omega}',\lambda')f_j^{(n-1)}(\tau,\vec{\omega}',\lambda')\end{aligned} \tag{2.79}$$

with source function

$$f_i^{(0)}(z,\vec{\omega},\lambda) = \frac{1}{2|\eta|} S_i(\vec{\omega},\lambda)(1 + \text{sgn}\ \eta\ \text{sgn}\ z)\exp\left(-\frac{\mu|z|}{|\eta|}\right) \tag{2.80}$$

and with (i, $j = I$, Q, U, V). The overall intensity is obtained (component by component) by adding the contributions from the different numbers of collisions, as for the scalar model:

$$I_i(\vec{\omega},\lambda) = |\eta| f_i(0,\vec{\omega},\lambda) = |\eta| \sum_{k=0}^{\infty} f_i^{(k)}(0,\vec{\omega},\lambda) \tag{2.81}$$

as shown in Figure 2.12.

2.4.3 DIFFERENCES AND SIMILARITIES BETWEEN THE SCALAR AND VECTOR MODELS

From a mathematical point of view, the only apparent difference between Eqn (2.73) and the scalar equation for average polarized radiation, Eqn (2.69), is the vectorial character of Eqn (2.73). The similarity between these equations is deeper because both are linear equations, which ensures that an overlapping of source terms will produce a corresponding overlapping of solutions. This strong property supports the idea of computing orders-of-interaction solutions for both equations.

The many new ideas introduced by Eqn (2.73) are responsible for the substantial differences between the solutions of both equations.

First, we obtain the four coupled equations (2.78) which give the Stokes components of the intensity. These components are used to determine how the state of polarization changes after every collision, and therefore they give richer information about the whole transport process. The first Stokes component represents the detected intensity, and corresponds to the solution of the scalar equation. Although the vector equation is linear, the single equation for the intensity is non-linear due to the coupling terms. This fact has two important consequences. In the first place, it is not possible to solve the equation for the intensity separately, without considering the other coupled equations. This prevents against looking for a solution for this single scalar equation, without considering the evolution of the full polarization state (even using Monte Carlo methods). In the second place, the solution obtained for the intensity differs from that predicted with the scalar equation for unpolarized excitation, except for the first collision which gives the same result in both cases. For polarized excitation the intensity has been calculated using the whole vector equation, and therefore a direct comparison with solutions of some scalar equation using polarization-dependent kernels has been not possible. However, it has been shown that for the case of linear polarization it is not possible to establish a parallelism between both types of solutions, scalar and vector, because the coupling of the flux components in Eqn (2.73) produces only new states of

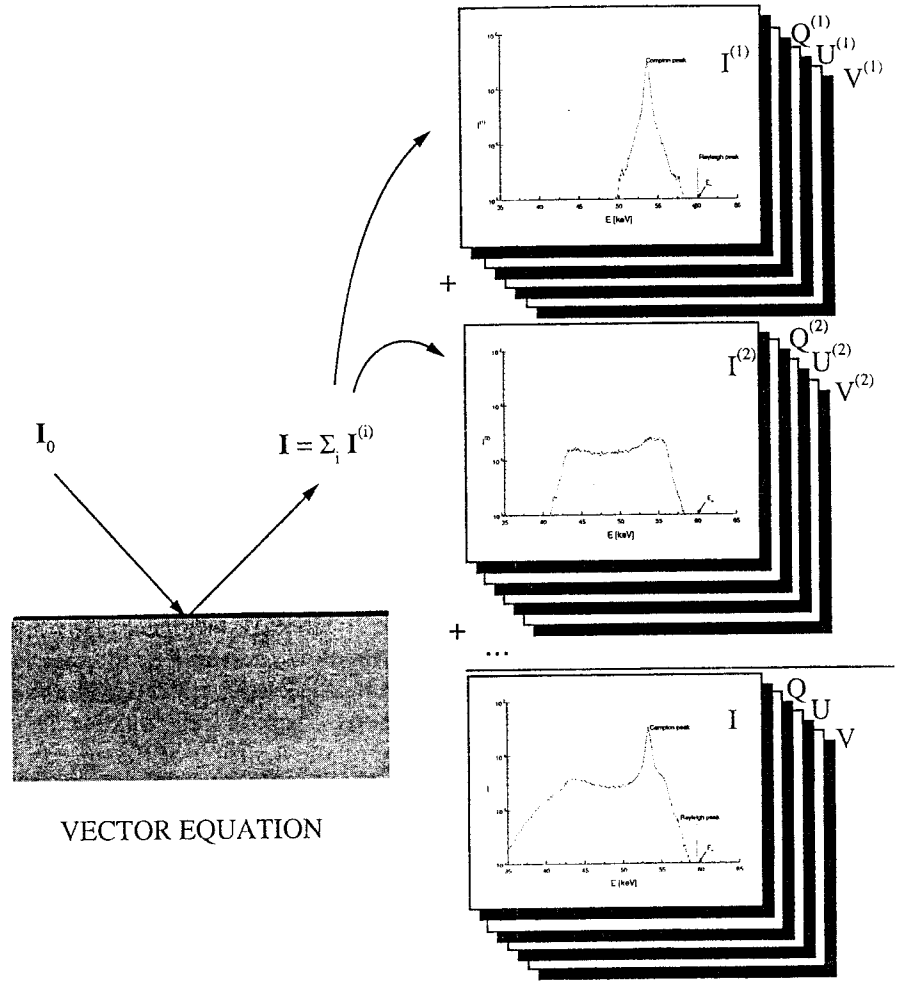

Figure 2.12 Diagram of the orders-of-interaction solution obtained with the vector equation. Each number of collisions contributes a term to the overall spectrum. All the terms are formed by the four components of the Stokes intensity. This makes it possible to determine the contribute of every term to the state of polarization of the spectrum as a function of the energy. Every term can be split again into the contributions involving the different collision chains of the participating interactions.

linear polarization for scattering collisions (with electrons having randomly oriented spins, i.e. for non-magnetic states of the matter). This allows us to hypothesize that Monte Carlo programs [91–93] using scalar (but polarization-dependent) differential cross-sections, cannot produce equivalent results to the vector solution because they are not able to describe appropriately (i.e. at every collision) the exchange between polarized and unpolarized states

produced by the scattering events. A formal demonstration has been given by showing that the scalar problem would require a non-linear transport equation to reach the results obtained with the (linear) vector equation in the case of an unpolarized source [97].

For matter under an external magnetic field, the Compton matrix kernel has non-zero matrix components in the last row and column that create non-linear components of polarization in each collision [71]. This condition prevents the use of the scalar model of transport. Besides the well known magnetic behavior of Compton scattering, similar behavior for Rayleigh scattering has also been reported by Simon and Daniel [94]. For non-linear polarization of the incident beam (circular polarization for instance), the requirement is similar to that for the linear polarization case. In the absence of an external magnetic field the last equation in Eqn (2.78) (i.e. corresponding to $f_v(\vec{r}, \vec{\omega}, \lambda)$) is not coupled, and the vector equation can be reduced of one dimension. For a magnetic field, in contrast, it is mandatory to use the full vector model of transport.

Second, the fact that rotations that appear in Eqn (2.74) modify the angular dependence of the kernel $\mathbf{K}^{(s)}(\vec{\omega}, \lambda, \vec{\omega}', \lambda')$, is very important. Indeed, the kernel $\mathbf{K}^{(s)}$ in the local-centre-of-mass system, due to the symmetry of the collision, depends on the scattering angle but not on the direction of incidence. This is a very intuitive result that can be easily verified on all the scattering processes in the X-ray regime. Mathematically, this means that the kernel will depend on the scalar product $\vec{\omega} \cdot \vec{\omega}'$ and not on the directions $\vec{\omega}$ or $\vec{\omega}'$ individually. This property can be understood as a consequence of the isotropy of the space in which the collision undergoes. However, for the kernel $\mathbf{H}^{(s)}$ appearing in the transport Eqn (2.73), $\mathbf{K}^{(s)}$ is the kernel after the two rotations shown in Eqn (2.74). These rotations destroy the kernel dependence on $\vec{\omega} \cdot \vec{\omega}'$, and make it dependent on $\vec{\omega}$ and $\vec{\omega}'$ separately. In other words, these rotations destroy the isotropy of the space and make the angular distribution, produced as a consequence of the scattering processes, appear deformed with respect to the original distribution in the local-centre-of-mass system. An example of this property is shown in Figure 2.13.

The last consideration concerns the influence of polarization on the different types of interactions in the X-ray regime. The Rayleigh and Compton scattering processes are strongly dependent on the polarization, whereas the transitions that fill the photoelectric vacancies are almost independent of it. Multiple collisions will mix the effects of the polarization on the single participating collisions. In this way, multiple collisions involving the photoelectric effect, preceded by a scattering collision, will also bring the effect of the polarization to the characteristic lines. Under these circumstances, there is no one part of the X-ray spectrum that remains completely independent of the polarization state of the source.

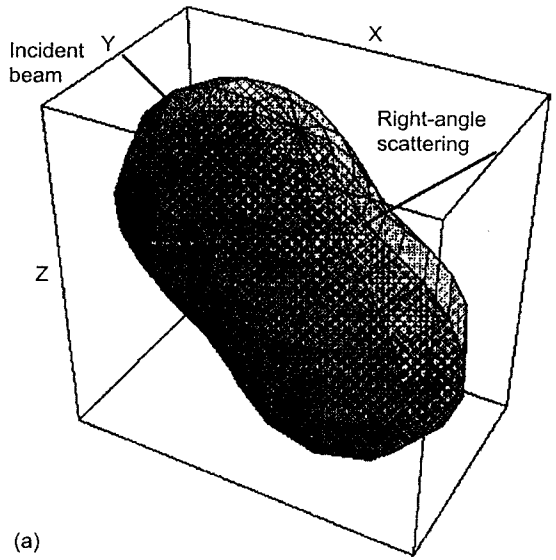

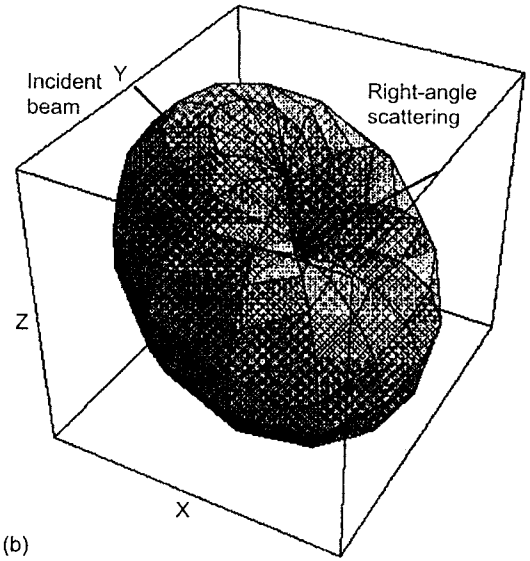

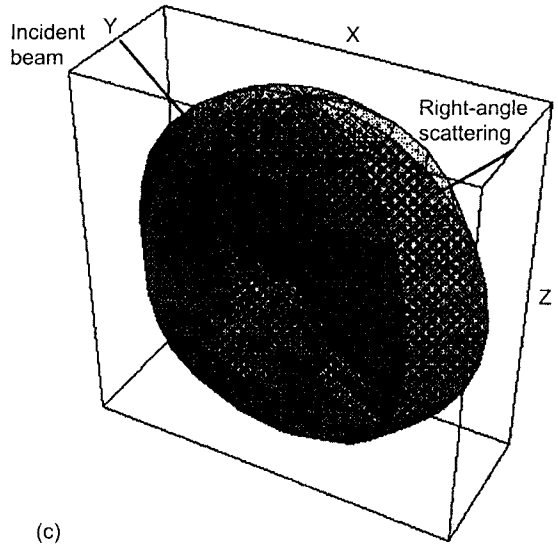

Figure 2.13 Iso-intensity surfaces illustrating the angular dependence of the first-order intensity of Rayleigh scattering for unpolarized and linearly polarized sources with different orientations of the electric vector: (a) unpolarized beam (intensity shows azimuthal symmetry around the incidence direction); (b) linearly polarized in the x–z plane (the intensity is null for the scattering direction, and a maximum on a normal plane to it); (c) linearly polarized along y (intensity is maximum in the x–z plane and null on the y axis).

2.5 Interpretation of X-ray fluorescence spectra

In XRF and SRXRF of thick samples, the whole X-ray spectrum receives important contributions from multiple collisions of interactions, such as the photoelectric effect, Rayleigh scattering and Compton scattering, which depend differently on the polarization state of the incoming photons. Three groups of multiple scattering contributions appear clearly in the spectrum: pure photoelectric, pure scattering and photoelectric–scattering. The pure photoelectric group produces the essential part of the characteristic lines. The pure scattering group creates a continuous background which starts from the excitation energy and goes towards lower energies. Besides producing the well known broadening of the Compton peak (Compton profile), the momentum distribution of the atomic electrons renders possible the so-called inverse Compton effect, i.e. the Compton tail extends up to energies (slightly) higher than the excitation energy. The photoelectric–scattering group overlaps discrete and continuous enhancements to the characteristic lines, modifying appreciably their intensity and shape especially under certain conditions of excitation and sample composition. As the photoelectric effect is less influenced by the polarization state than the scattering processes, the line spectrum produced with a synchrotron looks quite similar to that produced

with a conventional X-ray tube, under equivalent conditions of monochromaticity and geometrical set-up. On the contrary, the pure scattering background can be substantially reduced with an appropriate choice of polarization direction of the synchrotron beam, giving a better signal-to-noise ratio and, therefore, improving the detection limits of the elements present. The photoelectric–scattering contribution is also reduced by the effect of the polarization, but is not canceled. The reduction is less evident than for pure scattering because the presence of the photoelectric effect in the collision chains decreases the sensitivity to polarization. The apparent similarity of the line spectra has induced the analysts to consider the cleaner spectrum from a polarized source as being free of the scattering interferences inherent to conventional sources. Such assumptions are erroneous and may introduce an appreciable error in trace element analysis if the phototelectric–scattering contribution is neglected [95].

The effects of the polarization have received growing attention from two different points of view, transport calculations and Monte Carlo statistical simulation. Both approaches descend from transport theory and allow the use of detailed cross-sections for describing the single interactions. On the one hand, transport calculations have the theoretical advantage of offering analytical expressions for many terms of multiple scattering, allowing an in-depth study of the intensities in relation to the multiple parameters influencing them, from the energy and the set-up, to the arbitrary polarization state of the source. On the other hand, Monte Carlo simulation offers the possibility of computing higher-order terms of multiple scattering intensity without the comprehensible restrictions on the model geometry associated with the transport calculations. The two methods are equivalent and complementary provided that rigorous Monte Carlo, able to describe correctly the evolution of the polarization state, is used for the simulation.

2.5.1 ADVANTAGES AND LIMITATIONS OF THE TRANSPORT MODEL FOR DESCRIBING X-RAY DIFFUSION

The vector model of photon transport gives a rigorous description of the fluorescence of photons produced with a source of arbitrary polarization. The information obtained on the multiple scattering terms is not only circumscript to the intensity. It involves the full polarization state as a function of the energy, and of the incidence and take-off angles. The supplementary information is very rich and allow us to hypothesize the possibility of performing polarimetric X-ray spectrometry, by inserting a polarization analyzer before the detector.

The three prevailing processes in the X-ray regime (photoelectric effect, Rayleigh scattering and Compton scattering) are considered in great detail and are described by state-of-art matrix kernels. These expressions, valid for multicomponent targets with elements from hydrogen to uranium, enable us to obtain accurate intensity expressions for many multiple scattering terms produced by polarized sources (Table 2.1).

Table 2.1 Classification of the multiple scattering intensity terms, by groups. Reprinted from Ref. 95 by courtesy of Marcel Dekker Inc.

Number of collisions	Term nomenclature	Type	Meaning	Intensity for differently polarized sources[a]		
				Unpolarized	Linearly polarized	Circularly polarized
Pure photoelectric group						
1	(P)	Discrete[b]	Primary intensity of the characteristic line: only the atoms of the same element can contribute to the characteristic lines of the element. Therefore, this is the only intensity term that, for monochromatic excitation, can be transformed in a linear function of the concentrations.	Eqn (13a)[e]	Eqn (13a)[e]	Eqn (13a)[e]
2	(P,P)	Discrete[b]	Secondary intensity of the characteristic line: is considered the main enhancement to the primary intensity. This kind of contribution involves, usually, characteristic emission from two atoms of different elements and, therefore, is associated with multi-element samples. Frequently, there are several terms of these for each line, all strongly non-linear as a function of the concentrations, as in the case of monochromatic excitation.	Eqn (13b)[e]	Eqn (13b)[e]	Eqn (13b)[e]
3	(P,P,P)	Discrete[b]	Tertiary intensity of the characteristic line: is usually considered a minor enhancement of the primary intensity. This contribution involves, usually, characteristic emission from three atoms of different elements, and therefore, is associated with multi-element samples. These terms are strongly non-linear as a function of the	Eqn (13c)[e]	Eqn (13c)[e]	Eqn (13c)[e]

Table 2-1 (Contd.)

			concentrations, as in the case of monochromatic excitation. Although the single tertiary terms are small (roughly, 10^{-1} of a secondary term), the number of terms can be very large for certain lines. This fact can render the contribution important			
4	(P,P,P,P)	Discrete[b]	Fourth-order intensity of the characteristic line: is usually considered a minor enhancement of the primary intensity. This contribution involves, usually, characteristic emission from four atoms of different elements, and therefore, is associated with multi-element samples. These terms are strongly non-linear as a function of the concentrations, as in the case of monochromatic excitation. Although each single fourth-order term is small (roughly, 10^{-2} of a secondary term), in targets with many elements the number of terms can be very large for certain lines. This fact can render the contribution important.	Eqn (6)[f]	Eqn (6)[f]	Eqn (6)[f]
higher	ALL	Discrete[b]	Presumably not significant	NA[h]	NA	NA
Pure scattering group						
1	(R)	Discrete[c]	Rayleigh scattering of the source beam (also known as Rayleigh line, in case of monochromatic excitation). More important in light elements, and at low excitation energies. This scattering contribution can be appreciable for polychromatic excitation. Is strongly dependent on the polarization state of the source.	Eqn (58)[g]	Eqn (73e)[g]	Eqn (58)[g]

Table 2.1 (Contd.)

Number of collisions	Term nomenclature	Type	Meaning	Intensity for differently polarized sources[a]		
				Unpolarized	Linearly polarized	Circularly polarized
1	(C)	Continuous[d]	Compton scattering of the source beam (also known as Compton line, in case of monochromatic excitation). Is more important in light elements, and at high excitation energies. This scattering contribution can be appreciably high for both, monochromatic and polychromatic excitation. It can overlap characteristic lines. Is strongly dependent on the polarization state of the source.	Eqn (59)[g]	Eqn (74f)[g]	Eqn (59)[g]
2	(R,R)	Discrete[c]	Double Rayleigh scattering of the source beam: is the main enhancement of the Rayleigh line. In general, it is greater for light elements and low excitation energies, but has small absolute importance. It is strongly dependent on the polarization state of the source.	Eqn (60a)[g]	Eqn (75a)[g]	Eqn (60a)[g]
2	(C,C)	Continuous	Double Compton scattering of the source beam. Is the most intense two-collisions term in this group. Gives the characteristic continuous plateau under the Compton peak, which extends from $E_0/(1+2(E_0/511)(1+\cos(\Theta/2)))$ to $E_0/(1+2(E_0/511)(1-\cos(\Theta/2)))$, where Θ is the scattering angle. It is strongly dependent on the polarization state of the source.	Eqn (61a)[g]	Eqn (76a)[g]	Eqn (61a)[g]

Table 2-1 (Contd.)

2	(C,R)	Continuous	Double scattering Compton-Rayleigh. Is a peaked contribution, with its maximum coincident with the Compton energy, which extends from $E_0/(1+2(E_0/511))$ to E_0. It is strongly dependent on the polarization state of the source.	Eqn (63a)[g]	Eqn (78a)[g]	Eqn (63a)[g]
2	(R,C)	Continuous	Double scattering Rayleigh-Compton. Peaked contribution, with the maximum at the Compton energy, which extends from $E_0/(1+2(E_0/511))$ to E_0. Strongly dependent on the polarization state of the source.	Eqn (62a)[g]	Eqn (77a)[g]	Eqn (62a)[g]
3	ALL	Continuous	The third-order scattering spectrum goes from $E_0/(1+2(E_0/511)(2+\cos(\Theta/2)))$ to E_0. It is important for light samples ($Z < 20$). It is strongly dependent on the polarization state of the source.	MC[i]	MC	MC
4	ALL	Continuous	The fourth-order scattering spectrum goes from $E_0/(1+2(E_0/511)(3+\cos(\Theta/2)))$ to E_0. It is important for very light samples ($Z < 10$). It is strongly dependent on the polarization state of the source.	MC	MC	MC
higher	ALL	Continuous	Not significant, except for very light elements.	MC	MC	MC
Photoelectric-scattering group						
2	(P,R)	Discrete[b]	Characteristic X-rays, Rayleigh scattered in the target towards the detector. This term is the main scattering enhancement in heavy elements. In light elements it prevails only for low excitation energies. Does not depend on the polarization state of the source.	Eqn (55)[g]	Eqn (55)[g]	Eqn (55)[g]

Table 2.1 (Contd.)

Number of collisions	Term nomenclature	Type	Meaning	Intensity for differently polarized sources[a]		
				Unpolarized	Linearly polarized	Circularly polarized
2	(R,P)	Discrete[b]	Characteristic X-rays produced by Rayleigh scattered source beam photons. Less intense than the (P,R) term, except in very light elements for medium excitation energies. Is strongly dependent on the polarization state of the source.	Eqn (53)[g]	Eqn (71a)[g]	Eqn (53)[g]
2	(C,P)	Discrete[b]	Characteristic X-rays produced by Compton scattered source beam photons. This term is the dominant scattering enhancement in light elements at high excitation energies, but is low in heavy elements. Is strongly dependent on the polarization state of the source.	Eqn (56)[g]	Eqn (72a)[g]	Eqn (56)[g]
2	(P,C)	Continuous	Characteristic X-rays, Compton scattered in the target towards the detector. Negligible in light elements, becomes more significant in heavy elements although never exceeds a few percents of the primary intensity. Is a continuous contribution (from $E_i/(1 + 2(E_i/511))$ to E_i), modifying the symmetry (and shape) of the characteristic line. Does not depend on the polarization state of the source.	Eqn (57)[g]	Eqn (57)[g]	Eqn (57)[g]

Table 2-1 (Contd.)

3	ALL	Continuous	The third-order scattering spectrum extends from $E_i/(1 + 4(E_i/511))$ to E_i. Is significant only for light samples ($Z < 20$). Is dependent on the polarization state of the source.	MC[i]	MC	MC
higher	ALL	Continuous	Not significant	MC	MC	MC

[a] The calculation methods mentioned in the three columns are for a target in the absence of an external magnetic field. The geometrical set-up is the usual 135°/45°/0°/0° (corresponding to incidence and take-off polar angles of 45°). All the equations mentioned are valid for monochromatic sources. For polychromatic excitation, the intensity must be multiplied by the excitation spectral density and integrated between its wavelengths limits. The referenced equations correspond to pure element targets, but can be easily modified for multi-element collisions.
[b] Except for the natural width of the line.
[c] Within the monochromaticity of the excitation beam. For SRXRF, the monochromaticity is typically $10^{-2} - 10^{-4}$.
[d] The continuous spectrum is the Compton profile.
[e] [21]
[f] [96]
[g] [90]
[h] NA
[i] MC

Photons from bremsstrahlung of secondary electrons (Compton or photoelectrons) are not considered, but this limitation is not severe within the energy regime considered here (and is common to many Monte Carlo codes, too).

These characteristics make the transport model particularly appropriate for the analytical study of multiple scattering intensity terms which, overlapped, build up the total X-ray spectrum. In general, the multiple scattering contributions can be classified in relation to (i) the affiliation to one of the three groups of contributions mentioned above, (ii) the number of collisions, (iii) the intervening processes, (iv) the kind of intensity contributed to the X-ray spectrum (discrete or continuous), (v) the method used for the computation, and (iv) how they depend on the polarization state of the source photons. A classification scheme containing these characteristics of the multiple scattering terms is shown in Table 2.1 for monochromatic excitation, in absence of external magnetic fields near the target. The table reports the references and equation numbers of the analytical descriptions (in the frame of transport theory) found in the literature for the most intense terms. The terms which have never been calculated analytically but have been estimated with Monte Carlo simulation, are marked MC. If no computation is known, the term is marked as not available (NA).

2.5.2 EXAMPLE

To exemplify the complex influence of the polarization a test sample dilution of Ho (0.1%) in water (99.9%) was selected. Calculations were performed on this sample with both unpolarized and linearly polarized excitation beams and the results compared. The simulated spectra are shown, respectively, in Figures 2.14 and 2.15. The geometry in all cases was assumed as corresponding to incidence and take-off polar angles of 45°. The excitation energy was assumed to be 59.54 keV (equivalent to the energy of the most intense line of ^{241}Am).

The spectrum for the unpolarized beam (Figure 2.14) shows the contributions of the three groups mentioned. The black color corresponds to the pure photoelectric group. This is the only part in the spectrum that can be assumed to be completely independent of the polarization state of the source. The dark gray denotes the pure scattering group, which contains the Compton and Rayleigh peaks, plus the multiple scattering of these processes. We can see that the multiple scattering tail overlaps the Ho Kα_1 line, while the Compton peak overlaps the K$\beta_{1,3}$ line. The effect of the scattering is very different in the two cases. In the first, the contribution of the scattering part amounts to roughly 10% of the photoelectric part of the line. In the second case, the scattering is more than 600% of the photoelectric part, producing a huge interference. The light gray denotes the photoelectric–scattering contribution which is always present in all the lines. The influence of this contribution varies greatly for the different lines shown in the figure. It is very important for Kα_1

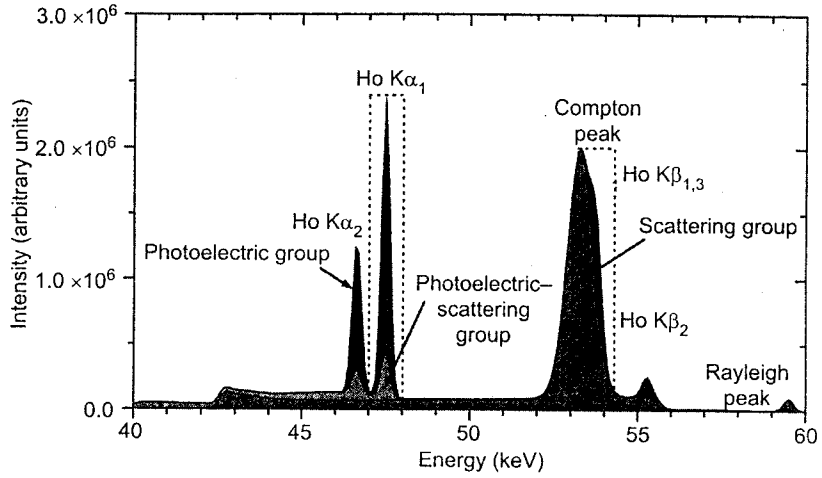

Figure 2.14 X-ray spectrum for a binary mixture of Ho (0.1%)–water (99.9%) calculated for unpolarized excitation. The source energy is 59.54 keV, and the incidence and take-off angles are 45° Reprinted from Ref. 95 by courtesy of Marcel Dekker Inc.

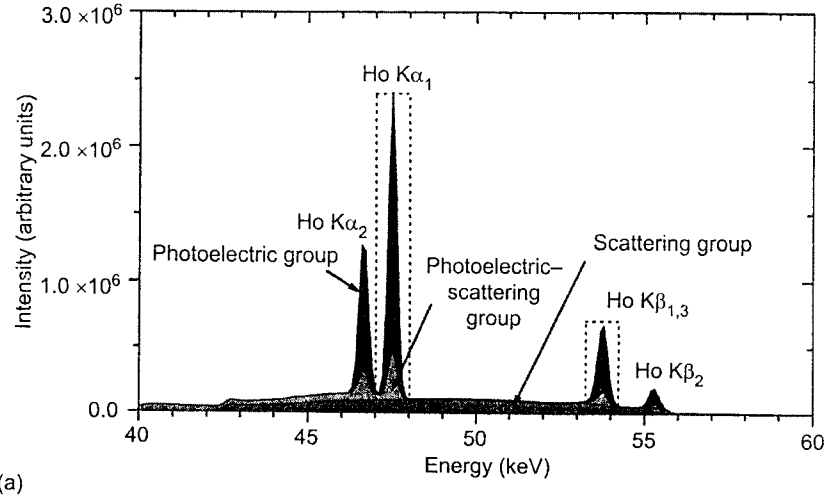

(a)

Figure 2.15 See page 58.

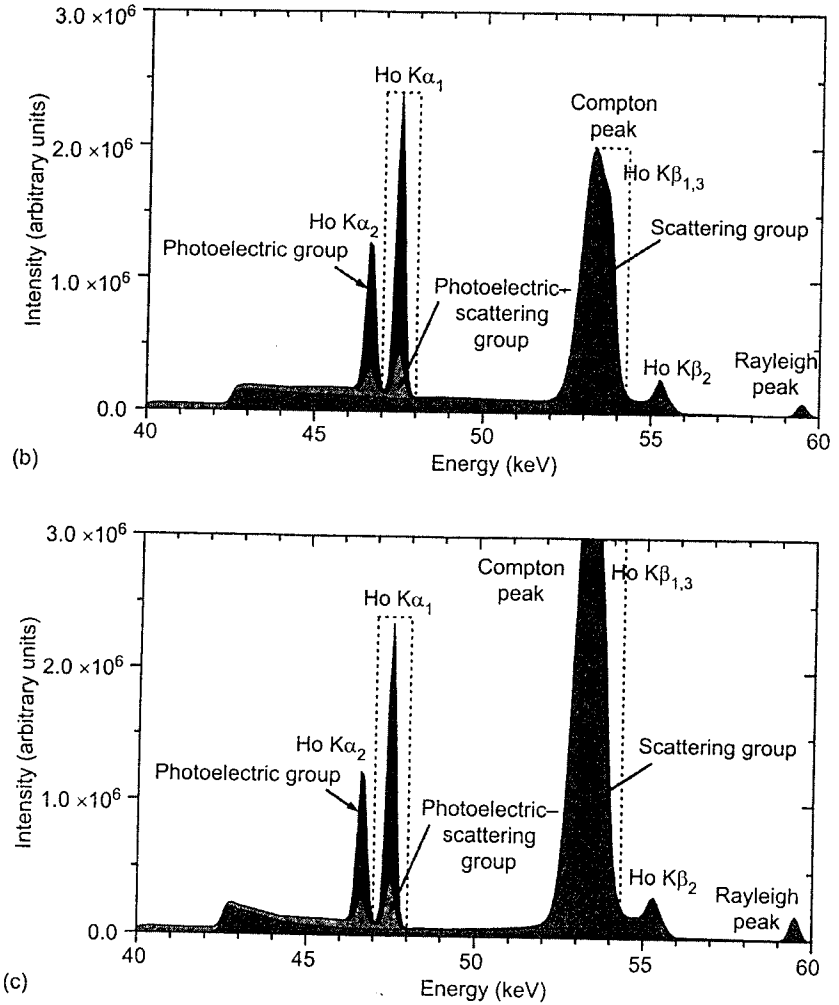

Figure 2.15 X-ray spectrum for a binary mixture of Ho (0.1%)–water (99.9%) calculated for linearly polarized excitation with three orientations of the electric field vector with respect to the scattering plane: (a) 0°; (b) 45°; (c) 90°. The source energy is 59.54 keV. The incidence and take-off angles are 45°Reprinted from Ref. 95 by courtesy of Marcel Dekker Inc.

and $K\alpha_2$ lines, but has little effect on the $K\beta_{1,3}$ and $K\beta_2$ lines. The reason is that Compton enhancement is not possible for these two lines.

Figures 2.15(a)–(c) show the spectra for linearly polarized excitation at three different orientations of the electric field vector with respect to the scattering plane (0°, 45° and 90°, respectively). Figure 2.15(a) ($\chi = 0°$) provides the best suppression of the Compton peak, that allows discovery of the magnitude of

the $K\beta_{1,3}$ line (compared with the other lines), but increases the multiple scattering background under the $K\alpha_1$ and $K\alpha_2$ lines. Figure 2.15(b) ($\chi = 45°$) gives a quite similar spectrum to the unpolarized case, except the more intense tail of the scattering group under the $K\alpha_1$ and $K\alpha_2$ lines. Figure 2.15(c) ($\chi = 90°$) gives the best background reduction under the $K\alpha_1$ and $K\alpha_2$ lines, but it also amplifies the Compton peak under the $K\beta_{1,3}$ line.

The contribution of the photoelectric–scattering group is almost uniform in all these cases. The reason is that two of the four contributions are independent of the polarization state of the source (see Table 2.1) and do not vary with the different polarization states. The other two contributions, (R, P) and (C, P), although dependent on the polarization, are scarecely sensitive to it.

References

[1] Evans R. D., *The Atomic Nucleus*, McGraw-Hill, New York (1955).

[2] Jauch J. M. and Rohrlich F, *The Theory of Photons and Electrons*, Springer-Verlag, Berlin (1976).

[3] Agarwal B. K., *X-ray Spectroscopy*, 2nd edn, Springer-Verlag, Berlin (1991).

[4] McMaster W. H., Kerr del Grande N., Mallett J. H. and Hubbell J. H. Compilation of X-ray Cross-sections, in: *Lawrence Livermore National Laboratory Report UCRL-50174*, Sect. 2, Rev. 1 (1969).

[5] Storm E. and Israel H. I, *Nucl. Data Tables* **A7**, 565 (1970).

[6] Veigele W. J., *At. Data* **5**, 51 (1973).

[7] Hubbell J. H., Gerstemberg H. M. and Saloman E. B., Bibliography of Photon Total Cross-sections (attenuation coefficients) measurements 10 eV to 13.5 GeV, in: *National Bureau of Standards Report NBSIR*, 86–3461 (1986).

[8] Saloman E. B., Hubbell J. H. and Scofield J. H., *At. Data Nucl. Data Tables* **38**, 1 (1988).

[9] Cullen D. E., Chen M. H., Hubbell J. H., Perkins S. T., Plechaty E. F., Rathkopf J. A. and Scofield J. H. Tables and Graphs of Photon-Interaction Cross Sections from 10 eV to 100 GeV Derived from the LLNL Evaluated Photon Data Library (EPDL), in: *Lawrence Livermore National Laboratory Report UCRL-5400*, Vol. 6, Parts A and B, Rev. 4 (1989).

[10] Kissel L. and Pratt R. H., *Trans. Am. Nucl. Soc.* **55**, 199 (1987).

[11] Kane P. P., Kissel L., Pratt R. H. and Roy S. C., *Phys. Rep.* **140**, 75 (1986).

[12] Bui C. and Milazzo M, *N. Cimento*, **D11**, 655 (1989).

[13] Ribberfors R. and Berggren K. F., *Phys. Rev.* **A26**, 3325; *Phys. Rev.* **A29**, 3451 (1982).

[14] Stokes G. G., *Trans. Cambridge. Phil. Soc.* **9**, 399 (1852).

[15] Fano U. and Cooper J. W., *Rev. Mod. Phys.* **40**, 441 (1968).

[16] Starace A. F., Theory of Atomic Photoionization, in: *Handbuch der Physik*, Vol XXXI, p. 1. Springer-Verlag, Berlin (1982).
[17] Amusia M. Y., *Atomic Photoeffect*, Plenum Press, New York (1990).
[18] Scofield J. H., *Trans. Am. Nucl. Soc.* **55**, 200 (1987).
[19] Scofield J. H., Theoretical photoionization cross-sections from 1 to 1500 keV, in: *Lawrence Livermore National Laboratory Report*, UCRL-51326 (1973).
[20] Bearden J. A., *Rev. Mod. Phys.* **39**, 78 (1967).
[21] Fernández J. E., *X-Ray Spectrom.* **18**, 271 (1989).
[22] Krause M. O. and Oliver J. H., *J. Phys. Chem. Ref. Data* **8**, 329 (1979).
[23] Salem S. I., Boehm F. and Lee P. L., *Nucl. Intrum. Methods Phys. Res.* **140**, 511 (1977).
[24] Fink R. W., Jopson R. C., Mark H. and Swift C. D., *Rev. Mod. Phys.* **38**, 513 (1966).
[25] Bambynek W., Craseman B., Fink R. W., Freund H. U., Mark H., Swift C. D., Price R. E. and Venugopala R. P., *Rev. Mod. Phys.* **44**, 716 (1972).
[26] Salem S. I., Panossian S. L. and Krause R. A., *At. Data Nucl. Data Tables* **14**, 91 (1974).
[27] Krause M. O., *J. Phys. Chem. Ref. Data* **8**, 307 (1979).
[28] Langenberg A. and Van Eck J., *J. Phys.* **B12**, 1331 (1979).
[29] Cohen D. D., *Nucl. Instrum. Methods Phys. Res.* **B22**, 55 (1987).
[30] Hubbell J. H., Bibliography and current status of K, L, and higher shell Fluorescence Yields for computation of Photon Energy-absorption Coefficients, in: *National Institute of Standards and Technology Report NISTIR*, 89–4144 (1989).
[31] Singh S., Mehta D., Garg R. R., Kumar S., Garg M. L., Singh N., Mangal P. C., Hubbell J. H. and Trehan P. N., *Nucl. Instr. Methods Phys. Res.* **B51**, 5 (1990).
[32] Puri S., Metha D., Chand B., Singh N. and Trehan P. N., *X-Ray Spectrom.* **22**, 358 (1993).
[33] Puri S., Metha D., Chand B., Singh N., Hubbell J. H. and Trehan P. N., *Nucl. Instr. Meth. Phys. Res.* **B22**, 21 (1993).
[34] Hubbell J. H., Trehan P. N., Singh N., Chand B., Metha D., Garg M. L., Garg R. R., Singh S. and Puri S., *J. Phys. Chem. Ref. Data* **23**, 339 (1994).
[35] Scofield J. H., *Phys. Rev.* **179**, 9 (1969).
[36] Scofield J. H., *Phys. Rev.* **A9**, 1041 (1974).
[37] Scofield J. H. Radiative Transitions in: *Atomic Inner Shell Processes*, Vol I, pp. 265–292 (B. Crasemann Ed.), Academic Press, New York (1975).
[38] Hansen J. S., Freund H. U. and Fink R. W., *Nucl. Phys.* **A142**, 604 (1970).
[39] Khan M. R. and Karimi M., *X-Ray Spectrom.* **9**, 32 (1980).
[40] Hubbell J. H., McMaster W. H., Kerr del Grande N. and Mallett J. H., X-ray Cross-sections and Attenuation Coefficients in: *International Tables for X-Ray Crystallography*, Vol. 4, p. 47, Kynoch Press, Birmingham (1974).

[41] Hubbell J. H., Gimm H. A. and Øverbø I., *J. Phys. Chem. Ref. Data* **9**, 1023 (1980).
[42] Hubbell J. H, *Int. J. Appl. Rad. Isot.* **33**, 1269 (1982).
[43] Trubey D. K., Berger M. J. and Hubbell J. H., Photon Cross Sections for ENDF/B-VI. in: *Advances in Nuclear Computation and Radiation Shielding*, April 9–13, Santa Fe (NM) (1989).
[44] Saloman E. B. and Hubbell J. H., *Nucl. Instrum. Meth. Phys. Res.*, **A255**, 38 (1987).
[45] Bearden J. A. and Burr F., *Rev. Mod. Phys.* **39**, 125 (1967).
[46] Flügge S., Mehlhorn W. and Schmidt V., *Phys. Rev. Lett.* **29**, 7 (1972).
[47] Kahlon K. S., Aulakh H. S., Singh N., Mittal R., Allawadhi K. L. and Sood B. S., *Phys. Rev.* **A43**, 1455 (1991).
[48] Papp T. and Campbell J. L., *J. Phys.* **B25**, 3765 (1993).
[49] Nelms A. T. and Oppenheim L., *J. Res. Nat. Bur. Stand.* **55**, 53 (1955).
[50] Hubbell J. H., Veigele W. J., Briggs E. A., Brown R. T., Cromer D. T. and Howerton R. J., *J. Phys. Chem. Ref. Data* **4**, 471 (1975).
[51] Hubbell J. H. and Øverbø I., *J. Phys. Chem. Ref. Data* **8**, 69 (1979).
[52] Schaupp D., Schumacher M., Smend F., Rullhusen P. and Hubbell J. H., *J. Phys. Chem. Ref. Data* **12**, 467 (1983).
[53] Veigele W. J., Tracy P. T. and Henry E. M., *Am. J. Phys.* **34**, 1116 (1966).
[54] Cromer D. T. and Waber J. T., *Acta Cryst.* **18**, 104 (1965).
[55] Cromer D. T. and Waber J. T., Atomic Cattering Factors for X-rays, in: *International Tables for X-Ray Crystallography*, (J. A. Ibers and W. C. Hamilton, Eds), Vol. 4, pp. 71–147, Kynoch Press, Birmingham (1974).
[56] Rose P. F. and Dunford C. L., *ENDF-102 Data Formats for the Evaluated Nuclear Data File ENDF-6*. Brookhaven National Laboratory Informal Report BNL-NCS-44945 (1990).
[57] Cullen D. E., *Nucl. Instr. Meth. Phys. Res.* **B101**, 499 (1995).
[58] Hanson A. L., *Nucl. Instrum. Meth. Phys. Res.* **A234**, 552 (1985).
[59] Brown G. E. and Mayers D. F., *Proc. Roy. Soc. London* **A234**, 387 (1956).
[60] Brown G. E. and Mayers D. F., *Proc. Roy. Soc. London* **A242**, 89 (1957).
[61] Compton A. H., *Phys. Rev.* **21**, 483 (1923).
[62] Evans R. D., The Compton effect, in: *Handbuch der Physik*, Vol XXXIV, p. 218. Springer, Berlin (1958).
[63] Klein O. and Nishina Y., *Z. Phys.* **52**, 853 (1929).
[64] Heitler W. *The quantum theory of radiation*, Clarendon Press, Oxford (1935).
[65] Waller I. and Hartree D. R., *Proc. R. Soc. London* **A124**, 119 (1929).
[66] Smith Jr. V. H., Thakkar A. J. and Chapman D. C., *Acta Cryst.* **A31**, 391 (1975).
[67] Cooper M. J., *Rep. Prog. Phys.* **48**, 415 (1985).
[68] Biggs F., Mendelsohn L. B. and Mann J. B., *At. Data Nucl. Data Tables* **16**, 201 (1975).
[69] Stroscio M. A., *Phys. Rev.* **A29**, 1691 (1984).

[70] Fano U., Spencer L.V. and Berger M. J., Penetration and diffusion of X-rays, in: *Encyclopedia of Physics*, Vol 38/2, p. 660. Springer Verlag, Berlin (1959).
[71] Fano U., *J. Opt. Soc. Am.* **39**, 859 (1949).
[72] Franz W., *Z. Physik* **98**, 314 (1936).
[73] Franz W., *Ann. Physik* **33**, 689 (1938).
[74] Lipps F. W. and Tolhoek H. A., *Physica* **20**, 85 (1954).
[75] Lipps F. W. and Tolhoek H.A., *Physica* **20**, 395 (1954).
[76] Tolhoek H. A., *Rev. Mod. Phys.* **28**, 277 (1956).
[77] Olsen H., Polarization Effects in Scattering and Radiation Processes, Chapter 4 in: *Applications of Quantum Electrodynamics*, Springer Tracts in Modern Physics, Vol. 44, p. 106. Springer-Verlag, Berlin (1968).
[78] Ewald H. and Franz W., *Z. Naturforsch.* **A31**, 808 (1976).
[79] Platzman P. M. and Tzoar N., *Phys. Rev.* **B2**, 3556 (1970).
[80] Platzman P. M. and Tzoar N., *J. Appl. Phys.* **57**, 3623 (1985).
[81] Collins S. P., Cooper M. J., Lovesey S. W. and Laundy D., *J. Phys.: Condens. Matter* **2**, 6439 (1990).
[82] Collins S. P., Laundy D. and Rollason A. J., *Phil. Mag.* **B65**, 37–46 (1992).
[83] Blume M., *J. Appl. Phys.* **57**, 3615 (1985).
[84] Blume M. and Gibbs D., *Phys. Rev.* **B37**, 1779 (1988).
[85] Gibbs D., Moncton D. E. and D'Amico K. L., *Appl. Phys.* **57**, 3619 (1985).
[86] Gibbs D., Blume M., Harshman D. R. and McWhan D. B., *Rev. Sci. Instr.* **60**, 1655 (1989).
[87] Cooper M. J., Zukowski E., Collins S. P., Timms D. N., Itoh F. and Sakurai H., *J. Phys.: Condens. Matter* **4**, L399 (1992).
[88] Timms D. M., Zukowski E., Cooper M. J., Laundy D., Collins S. P., Itoh F., Sakurai H., Iwazumi I., Kawata H., Ito M., Sakai N. and Tanaka Y., *J. Phys. Soc. Jpn*, **62**, 1716 (1993).
[89] Fernández J. E. and Molinari V. G., X-Ray Photon spectroscopy calculations, in: *Advances in Nuclear Science and Technology*, Vol. 22, p. 45, (J. Lewins and M. Becker Eds), Plenum Press, New York (1991).
[90] Fernández J. E., Hubbell J. H., Hanson A. L. and Spencer L. V., *Rad. Phys. Chem.* **41**, 579 (1993).
[91] Janssens K., Vincze L., Van Espen P. and Adams F., *X-Ray Spectrom.* **22**, 234 (1993).
[92] Namito Y., Ban S. and Hirayama H., *Nucl. Instr. Meth. Phys. Res.* **A332**, 277 (1993).
[93] Vincze L., Janssens K. and Adams F., *Spectrochim. Acta* **B48**, 553 (1993).
[94] Simon T. and Daniel H., *Phys. Rev.* **A15**, 1015 (1977).
[95] Fernández J. E., *J. Trace Microprobe Tech.* **14**, 489 (1996).
[96] Fernández J. E. and Molinari V. G., *Adv. X-Ray Anal.* **33**, 573 (1990).
[97] Fernández J. E., *Appl. Rad. Isot.* **49**, 83 (1998)

3 MICROFOCUSING X-RAY OPTICS

A. Rindby[1], F. Adams[2] and P. Engström[3]

[1]Department of Physics, Chalmers University of Technology, Sweden; [2]Department of Chemistry, University of Antwerp (UIA), Belgium; [3]European Synchrotron Radiation Facility, Grenoble, France

3.1 Introduction

In the past, X-ray fluorescence spectrometry has not been as widely applied at the microscopic level as the electron or proton microprobe techniques. This is due to the difficulties of optically controlling the X-ray beam as compared to a charged particle beam. Despite the fact that several different types of optical systems for focusing and imaging in the X-ray region have been developed, their efficiency is today still inferior to the conventional optical systems used for charged particles. This situation is now rapidly changing and high-intensity submicron size beams are becoming available through the various technological developments described in this chapter. However, even with poor optical efficiency, the X-ray microbeam offers many advantages for analysis and characterization in comparison with the other microprobe techniques, the major one being its higher analytical sensitivity. Chapter 7 provides a comparison of μ-XRF with other methods for microscopic analysis.

Whereas the electron lens system constructed in the early 1950s represented the starting point for a very rapid development of electron microscopy, X-ray microscopy and X-ray microbeam spectrometry did not develop at the same rate due to the practical difficulties in generating efficient optical systems for focusing X-rays. The requirement for microfocusing X-ray optics have been frequently formulated in the past, as have potential solutions to this problem. As early as 1936 Sievert [1] used a conventional aperture of a few micrometers to generate a small X-ray source for X-ray spectrometric applications. The lateral resolution thus obtained was adequate but the intensity was low. In 1939 von Ardenne [2] proposed an electron lens to generate small X-ray sources for projection-type X-ray microscopy. A microfocus X-ray tube based on the idea of von Ardenne was constructed by Cosslett and Nixon [3] in 1952. Kirkpatrick and Baez [4] mentioned the multiple X-ray refractive lens (the equivalent of the concave glass lens for visible light) in 1948 but concluded that such a device was unfeasible.

Microscopic X-ray Fluorescence Analysis. Edited by Koen H.A. Janssens, Freddy C.V. Adams and Anders Rindby © 2000 John Wiley & Sons Ltd. ISBN 0-471-97426-9.